

# Nanoparticle-Based Electrodes with High Charge Transfer Efficiency through Ligand Exchange Layer-by-Layer Assembly

Yongmin Ko, Cheong Hoon Kwon, Seung Woo Lee, and Jinhan Cho\*

Organic-ligand-based solution processes of metal and transition metal oxide (TMO) nanoparticles (NPs) have been widely studied for the preparation of electrode materials with desired electrical and electrochemical properties for various energy devices. However, the ligands adsorbed on NPs have a significant effect on the intrinsic properties of materials, thus influencing the performance of bulk electrodes assembled by NPs for energy devices. To resolve these critical drawbacks, numerous approaches have focused on developing unique surface chemistry that can exchange bulky ligands with small ligands or remove bulky ligands from NPs after NP deposition. In particular, recent studies have reported that the ligand-exchange-induced layer-by-layer (LE-LbL) assembly of NPs enables controlled assembly of NPs with the desired interparticle distance, and interfaces, dramatically improving the electrical/electrochemical performance of electrodes. This emerging approach also demonstrates that efficient surface ligand engineering can exploit the unique electrochemical properties of individual NPs and maximize the electrochemical performance of the resultant NP-assembled electrodes through improved charge transfer efficiency. This report focuses on how LE-LbL assembly can be effectively applied to NP-based energy storage/conversion electrodes. First, the basic principles of the LE-LbL approach are introduced and then recent progress on NP-based energy electrodes prepared via the LE-LbL approach is reviewed.

such as batteries, electrochemical capacitors (supercapacitors), and fuel cells.<sup>[1–8]</sup> Electrochemical energy storage devices can be categorized as Faradaic or non-Faradaic charge storage mechanisms depending on the presence of redox charge transfer reactions.<sup>[9]</sup> Various carbon materials (e.g., porous activated carbon, graphene, and carbon nanotubes (CNTs)) exhibit good charge transfer behavior (i.e., high power) due to their high electrical conductivity. In this case, the charged species (i.e., electric energy) are physically aligned and accumulate along the surface of carbon materials upon potential sweeps, forming an electrical double layer.<sup>[10]</sup> This charge storage mechanism, which is electrochemical double layer capacitance, has fast charge transfer kinetics and depends on the area of the electrode/electrolyte interface. However, these carbon materials with electrochemical double layer capacitance have intrinsically low-energy density (i.e., a low areal capacitance of  $\approx 30 \mu\text{F cm}^{-2}$ ),<sup>[11]</sup> limiting their use in high power applications, such as uninterruptible power supplies and

load leveling.<sup>[12]</sup> It has been reported that the immobilization of oxygen functional groups on the surface of carbon materials can induce a Faradaic reaction with specific cations (e.g.,  $\text{Li}^+$  or  $\text{H}^+$ ) and thus increase the energy density.<sup>[13,14]</sup> However, carbon-based electrodes have inherently low density ( $< 1 \text{ g cm}^{-3}$ ) and thus exhibit low volumetric energy density, limiting their practical use in high energy applications, including portable electronic devices and electric vehicles.

Recently, various transition metal oxides (TMOs), such as iron oxide, manganese oxide, cobalt oxide, and their mixed oxides, have been investigated for high energy density electrode materials for both pseudocapacitors and batteries due to their high theoretical capacity and large surface-to-volume ratio (i.e., large active surface area in nanomaterial-based electrodes).<sup>[15–23]</sup> That is, in contrast to capacitive carbon materials, TMO-based electrodes can store large amounts of energy through additional redox reactions ( $\approx 2.5$  electrons per metal atom of the accessible active surface of transition metal oxides<sup>[24]</sup>) on/near the electrode surface (pseudocapacitance) or within the bulk of the materials by ion intercalation or phase conversion reactions in battery systems.<sup>[25]</sup> In addition, the electrochemical performance of TMO-based electrodes can be further improved by controlling their structural parameters, such as particle size, uniformity, crystallinity, crystallite (domain) size, and orientation.<sup>[26–33]</sup>


## 1. Introduction

With the explosive growth of wearable, portable, and smart electronics for convenience and for enhancing the quality of daily life, numerous research efforts have been made to develop high-performance electrochemical energy storage/conversion systems

Dr. Y. Ko, Dr. C. H. Kwon, Prof. J. Cho  
Department of Chemical & Biological Engineering  
Korea University  
145 Anam-ro, Seongbuk-gu, Seoul 02841, Republic of Korea  
E-mail: jinhan71@korea.ac.kr

Dr. Y. Ko  
Division of Energy Technology  
Materials Research Institute  
Daegu Gyeongbuk Institute of Science and Technology (DGIST)  
333 Techno Jungang-daero, Hyeonpung-eup, Dalseong-gun  
Daegu 42988, Republic of Korea

Prof. S. W. Lee  
School of Mechanical Engineering  
Georgia Institute of Technology  
Atlanta, GA 30332-0245, USA

 The ORCID identification number(s) for the author(s) of this article can be found under <https://doi.org/10.1002/adma.202001924>.

DOI: 10.1002/adma.202001924

For example, a decrease in particle size from the micro- to nanoscale can shorten the ion diffusion and electron transfer length between adjacent active species within the electrode, thereby improving the rate performance of TMO-nanoparticle (NP)-based electrodes according to the following equation

$$L = \sqrt{Dt} \quad (1)$$

where  $L$ ,  $D$ , and  $t$  indicate the diffusion length within the electrode, the diffusion coefficient, and the specific time constant for ion diffusion, respectively. Furthermore, high crystallinity and an optimized crystallite size can enhance the structural stability under continuous electrochemical cycles as well as facilitate charge transport, resulting in a highly stable reversible capacity.<sup>[33,34]</sup> In this regard, high-quality (i.e., uniform particle size and high crystallinity) TMO NPs are a promising active component for high energy density electrodes in both pseudocapacitors and rechargeable batteries. Despite these advantages of TMO NPs, their relatively low electrical conductivity significantly restricts the energy storage efficiency under fast charge/discharge conditions, often resulting in poor rate performance. To resolve this issue, various physically blended nanocomposite electrodes composed of high-energy TMO NPs, carbon materials (as conductive enhancers), and polymer binders have been reported.<sup>[21–23,35–37]</sup> However, adding low-density carbon materials and electrochemically inactive polymer binders decreases the overall energy density of the electrode. Moreover, the organic ligands remaining on the surfaces of TMO NPs and the insulating polymer binders have a significant effect on the charge transfer between the active materials and thus increase the internal resistance of the electrodes. Therefore, it is highly desirable to control the structure of the electrodes, including the composition, packing density, and interfacial structure between the components, to exploit the intrinsic electrochemical properties of TMO NPs and maximize the electrochemical performance of the electrodes.

In the synthesis of inorganic NPs (including metal and TMO NPs), organic ligands are key components that control the shape of NPs and improve dispersion stability in solution-based electrode processes.<sup>[38–40]</sup> Additionally, the ligands remaining on the surface of the NPs can have a substantial effect on the ability to fully exploit the intrinsic electrical and electrochemical properties of the NPs,<sup>[41–45]</sup> which are directly related to the performance of various electrochemical devices prepared from NP-based electrodes. High-quality NPs are commonly synthesized in organic media using hydrophobic and bulky ligands (e.g., oleic acid (OA), palmitic acid (PA), and tetraoctylammonium bromide (TOA)). However, when using these NPs in electrodes for energy storage, the reported synthetic methods have the disadvantage that the insulating nature of these long aliphatic ligands can limit the charge transport at the NP/NP and/or NP/current collector interfaces. Thus, taking into account that NP-based electrodes for energy storage have a large interface area between components (i.e., the NP/NP and NP/current collector), fine-tuning the interfacial structure, including the effective removal and/or proper exchange of the insulating ligands on NPs, is essential to improve the performance of NP-based electrodes. In addition, it is desirable that this ligand engineering process should be ideally



**Yongmin Ko** received his Ph.D. degree at the Department of Chemical and Biological Engineering in Korea University in 2016. He was a postdoctoral researcher at Georgia Institute of Technology in Atlanta until 2019. Currently, he is working as a senior researcher at the Division of Energy Technology at the Daegu Gyeongbuk Institute of Science and Technology (DGIST) in Republic of Korea. His research interest is focused on energy conversion and storage devices based on various functional nanomaterials.



**Cheong Hoon Kwon** received her Ph.D. degree at the Department of Chemical and Biological Engineering in Korea University in 2008. She is a postdoctoral researcher at Harvard Medical School in Boston (in 2009–2010). In 2010–2015, she was a research professor in Hanyang University. Currently, she is a senior researcher at the Department of Chemical and Biological Engineering in Korea University. She has expertise in the surface modification of metal or metal oxide nanoparticles for electrochemical sensors (or actuators), biofuel cells, and energy storage devices. She has now focused on developing various energy electrodes using metal nanoparticle-based layer-by-layer assembly.



**Jinhan Cho** is a professor at the Department of Chemical & Biological Engineering in Korea University since 2010. His research career started in POSTECH and Seoul National University, where completed M.S. and Ph.D. degrees in 1997 and 2001, respectively. Then, he was a postdoc at Max Planck Institute of Colloids and Interfaces (in 2001–2002) and University of Melbourne (in 2003). In 2003–2005, he was a senior researcher in LG Chemistry R&D center. In 2006–2010, he had an academic career as an assistant professor at School of Materials Science and Engineering in Kookmin University. His research interests are now focused on studying the surface chemistry and electrochemical properties of various electrode materials, such as carbon nanotube, graphene, conducting polymer, and metal (or metal oxide) nanoparticle onto textile substrates.

performed under nondestructive and mild conditions to maintain the intrinsic properties of the active materials.

Numerous papers on ligand chemistry, including materials synthesis,<sup>[38,46]</sup> and ligand exchange processes,<sup>[47–49]</sup> have been reported to date. However, most studies have considered the ligand exchange process as a single event for NPs dispersed in organic or aqueous media, and the in situ ligand exchange reactions on NPs during the solution-based electrode assembly processes have been largely unexplored. Recently, it has been reported that various hydrophobic ligands on inorganic NPs (i.e., metal and TMO NPs) can be easily replaced by amine ( $-\text{NH}_2$ )-functionalized small ligands (or linkers) with a low molecular weight ( $M_w$ ) through in situ ligand exchange reactions during the solution-based electrode assembly process (Figure 1a).<sup>[50–57]</sup> The ligand exchange reaction is induced by the differences in the binding energies of ligands to NPs using a short-chain amine-functionalized ligand having a higher binding energy and a long-chain ligand attached to the NPs with a lower binding energy. Therefore, the short-chain ligands can replace the long-chain ligands on the NPs during the solution-based layer-by-layer (LbL) deposition process to assemble bulk electrode materials consisting of 3D interconnected nanoparticles through molecule linkers. Significantly, the effective ligand exchange reactions on the NP surface dramatically improve the charge transfer kinetics between neighboring NPs by reducing the distance between them (Figure 1b). This in situ ligand-exchange-induced LbL (LE-LbL) assembly method can be an effective approach to prepare NP-based electrodes with a controlled thickness, composition, and functionality onto various substrates, irrespective of the substrate size or shape.<sup>[50–53,57–60]</sup> Given that the structural properties, compositions, and interfacial structure between NPs significantly affect the energy performance of electrodes, the LE-LbL assembly approach can provide new insights into the study of the structure–property performance relationship of NP-based electrodes for energy storage.

In this report, we discuss the recent progress of NP-based electrodes for energy storage prepared via in situ LE-LbL assembly to achieve high charge transfer efficiency. Additionally, we demonstrate that this ligand engineering approach can be applied to a wide range of inorganic NPs from metal to TMO NPs. First, we introduce an in situ ligand exchange reaction and its mechanism of LE-LbL assembly for NP-based electrodes. Herein, the electrical and electrochemical properties of the resulting NP-based electrodes are also presented. We show that the in situ LE-LbL assembly of conductive metal NPs can be effectively used to fabricate current collectors with excellent electrical conductivity for various electrochemical energy systems. In the next section, NP-based electrodes for energy storage devices, such as lithium-ion batteries, electrochemical capacitors, and biofuel cells, prepared by ligand engineering are reviewed. Using the in situ LE-LbL assembly, we systematically assembled 3D nanocomposite electrodes consisting of various components, including metal NPs with conductive properties, TMO NPs with charge storage properties, and an enzyme with catalytic properties; the nanocomposite electrodes have a controlled composition, alignment, and interfacial structure for various electrochemical energy storage and conversion devices. Finally, this report briefly describes the importance and prospects of interfacial engineering for future energy devices.

## 2. Ligand Exchange Layer-by-Layer Assembly

### 2.1. Effect of Surface Ligands on Charge Transfer Kinetics

The kind of organic ligand bound to the surface of inorganic NPs seriously affects the electrical and electrochemical characteristics<sup>[61–64]</sup> in the formation of inorganic NPs, and these effects can be further intensified when these NPs are adsorbed onto substrates for the preparation of NP-based nanocomposite electrodes.<sup>[65,66]</sup> First, considering the electrical properties, bulky and hydrophobic ligands with long aliphatic chains result in high contact resistance (i.e., insulating barriers) between adjacent NPs within the electrodes, which significantly reduces the electron transport within the NP networks, resulting in low electrical conductivity in the nanocomposite electrodes.<sup>[38,67–70]</sup> Typically, the charge transport mechanism in electrical conductors (e.g., metal NP-based nanocomposites) can be described by three representative theories of electron hopping, quantum tunneling, and ohmic conduction, which strongly depend on the thickness of insulating barriers (i.e., the interdistance between separated ligands) of adjacent NPs.<sup>[71,72]</sup> Murray and co-workers reported that dried solid-state film electrodes based on Au NPs stabilized with long alkane chains exhibited relatively low electrical conductivity due to the high activation energy (due to the presence of bulky organic ligands) for electron tunneling between neighboring Au NPs.<sup>[73,74]</sup> That is, the organic ligands surrounding the NPs play a similar role as the dielectric capacitor, and they cause electron confinement with a low capacitance ( $\leq 10^{-18}$  F, depending on the thickness of the ligand shell), which restricts facile charge movements between neighboring Au NPs. These interparticle-distance-dependent charge conduction behaviors have been further systematically studied through low-frequency impedance spectroscopy measurements on metal NP-based nanocomposites.<sup>[75,76]</sup> Heath and co-workers found that the transition of insulator-to-metal conduction behavior occurs when the interparticle spacing (i.e., the ligand shell thickness) between adjacent metal NPs decreases to less than 6 Å. These phenomena have also been confirmed in various conductive noble metal and oxide NPs, silver,<sup>[66,68]</sup> copper,<sup>[77]</sup> aluminum,<sup>[78]</sup> tin and zinc oxide.<sup>[79–81]</sup> Additionally, Chen and co-workers reported that the electron transfer behavior is strongly influenced by the types of terminal moieties on ligands such as phenyl group-functionalized ligands.<sup>[82]</sup> That is,  $\pi$ - $\pi$  stacking of the phenyl groups can induce an overlap between adjacent ligands that can decrease the NP–NP interdistance, which increases charge transfer between neighboring NPs. They also demonstrated that the resulting charge transport characteristics show a clear Arrhenius behavior with a thermally activated hopping conduction mechanism.

Surface charge transfer kinetics at the interface also play a critical role in determining the electrochemical activity of NPs. In other words, the presence of bulky ligands covering the functional NPs can block the facile access of external reactive species (i.e., molecules, electrons, ions, and/or absorbates), thereby lowering the electrochemical activity of NPs and their composite electrodes.<sup>[45,83]</sup> Fan and co-workers reported that the catalytic activity of novel metal NPs (i.e., Pt, Pd, and Au NPs) could be notably improved by removing the native ligands through thermal annealing or electrochemical methods.<sup>[84,85]</sup> Specifically, as the surface coverage of polymeric ligands on

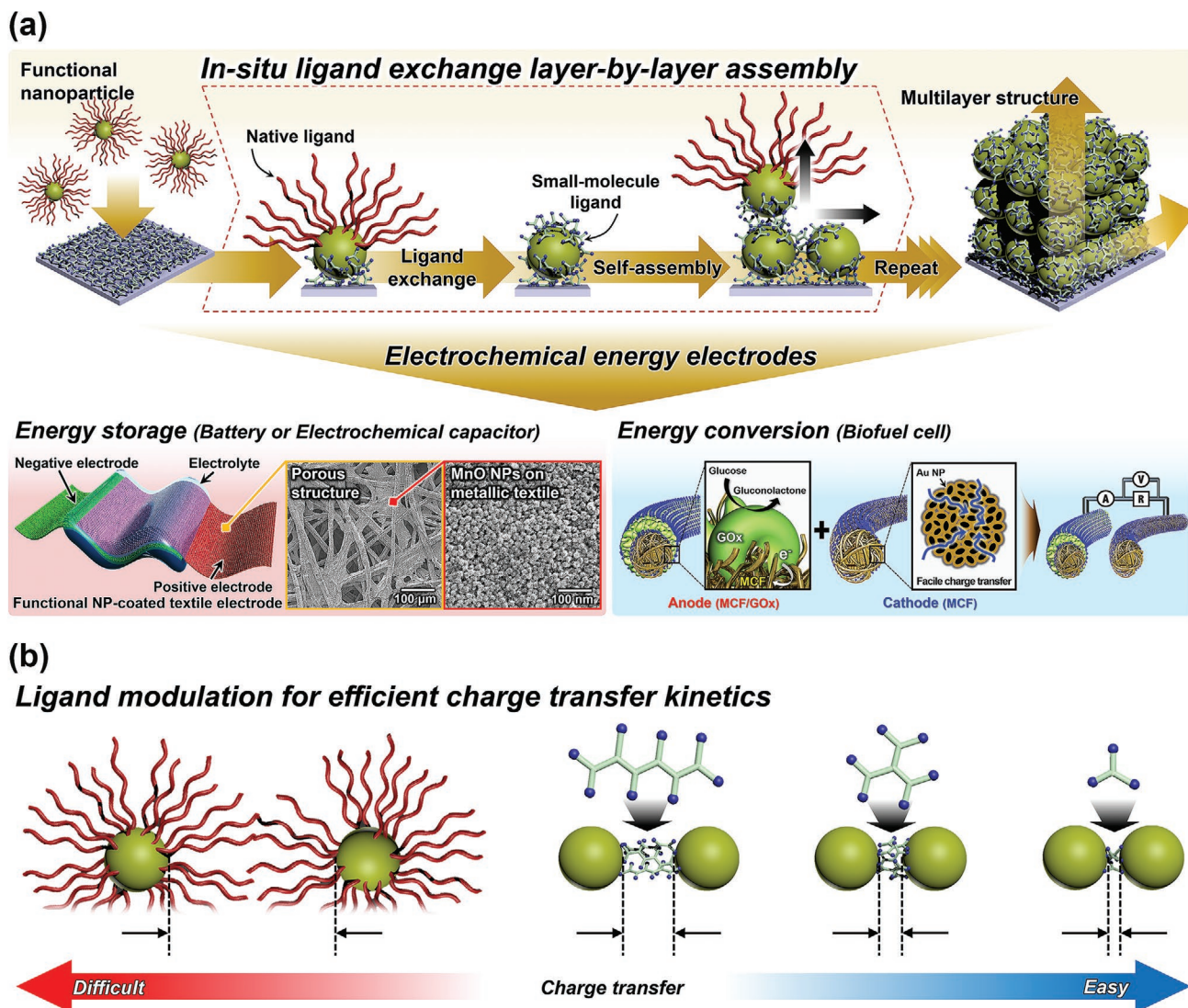


**Figure 1.** Schematic illustration of the preparation of nanoparticle-based electrodes for energy storage through ligand engineering. a) Schematic representation of the ligand-exchange-induced layer-by-layer (LE-LbL) assembly and its applications to electrochemical energy electrodes. Image for energy storage (bottom left): Adapted under the terms of the CC-BY Creative Commons Attribution 4.0 International license (<https://creativecommons.org/licenses/by/4.0/>).<sup>[52]</sup> Copyright 2017, The Authors, published by Springer Nature. Image for energy conversion (bottom right): Adapted under the terms of the CC-BY Creative Commons Attribution 4.0 International license (<https://creativecommons.org/licenses/by/4.0/>).<sup>[53]</sup> Copyright 2018, The Authors, published by Springer Nature. b) Schematic diagram of the ligand-dependent interparticle distance in the electrodes.

catalytic NPs decreased, the oxygen reduction reaction (ORR) activity and sensitivity of NPs gradually increased. These phenomena clearly indicate that organic ligands strongly affect the electrocatalytic properties of catalytic NPs as well as the electrical conductivity of metal NPs, as mentioned above.<sup>[86]</sup>

Likewise, the surface charge transport behavior of the TMO NPs can be controlled depending on the type or length of ligands (or linkers) on the NP surface.<sup>[87–90]</sup> In general, the insulating ligands coordinatively bonded through d-orbital participation with the transition metals limit the electron transport across NP networks. Cho and co-workers reported that the modulation of surface ligands on TMO NPs can increase the electrical and electrochemical properties.<sup>[87,88,91]</sup> The removal of bulky ligands (i.e., oleylamine (OAm)) bound to the surface of electrochromic

tungsten oxide ( $\text{WO}_{2.72}$ ) nanorods (NRs) enhanced the coloration efficiency (CE) and response time of coloration/bleaching cycles.<sup>[88]</sup> They also showed that the electrochemical (or electrochromic) performance of  $\text{WO}_{2.72}$  NR-based nanocomposites could be improved by reducing the ligand length or thickness of the ligand shell. That is, when small organic molecules were used as a linker instead of bulky polymers, the area in the cyclic voltammogram (CV) was notably increased with obvious reduction peaks at the same scan rate, which implied the significant influence of the ligands on electron transfer kinetics at the electrode interfaces (Figure 2a,b). This unique phenomenon could be further intensified by conductive TMO NPs such as indium tin oxide (ITO). As shown in Figure 2c,d, when OAm-ITO NP ligands were incorporated into  $\text{WO}_{2.72}$  NR-based

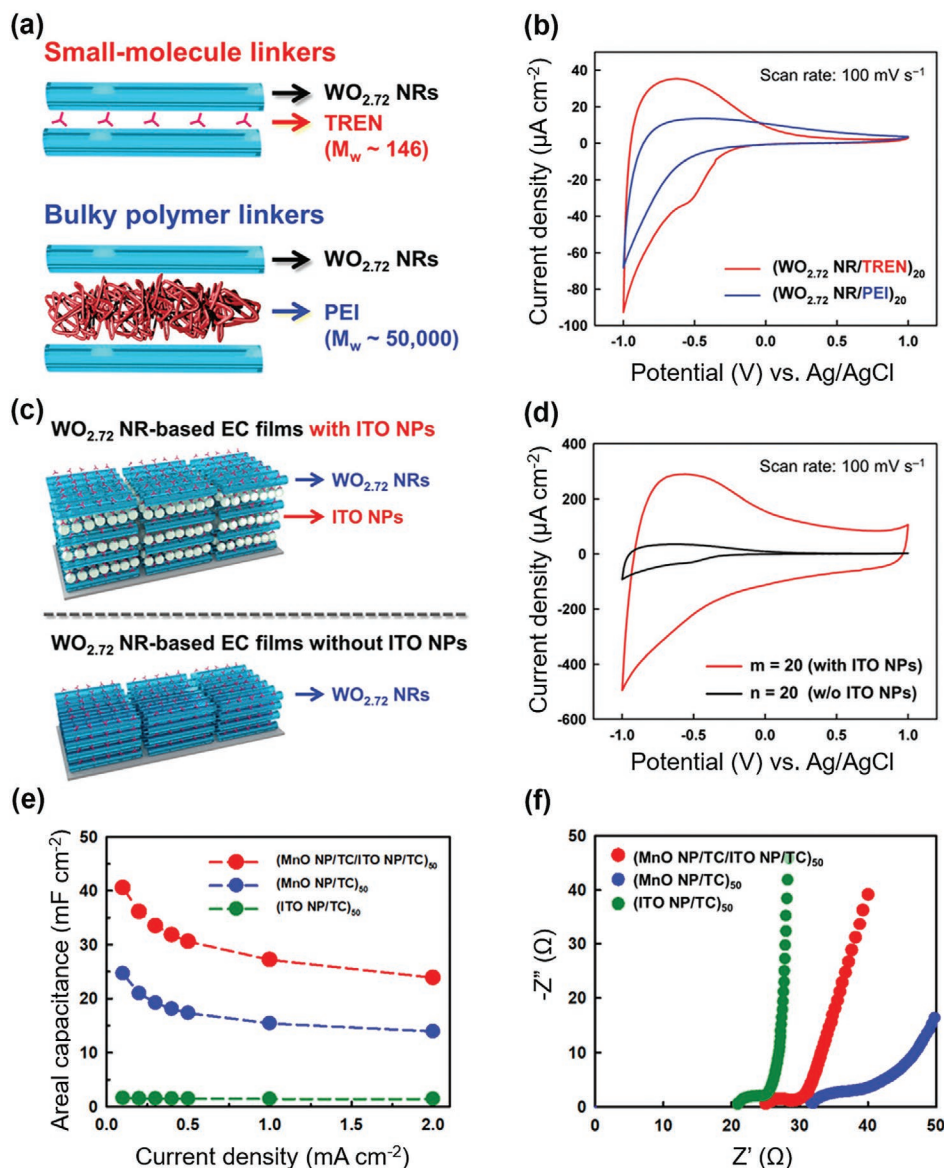


**Figure 2.** The role of the ligands in the electrochemical performance. a) Schematic illustration of  $\text{WO}_{2.72}$  NR-based film structures with different organic linkers (or different interdistances between  $\text{WO}_{2.72}$  layers). b) Cyclic voltammograms (CVs) of  $\text{WO}_{2.72}$  NR-based electrodes at  $100 \text{ mV s}^{-1}$  as a function of organic linker. c) Schematic illustration and d) CVs at  $100 \text{ mV s}^{-1}$  for  $\text{WO}_{2.72}$  NR-based electrodes with or without ITO NP layers. a–d) Adapted with permission.<sup>[88]</sup> Copyright 2019, The Royal Society of Chemistry. e, f) Comparison of the areal capacitance (e) and electrochemical impedance spectra (f) of MnO NP-based pseudocapacitor electrodes with or without an ITO NP layer. e, f) Adapted with permission.<sup>[91]</sup> Copyright 2019, American Chemical Society.

nanocomposites using LE-LbL assembly, the electrochemical responses in CVs were more notably improved compared to the electrodes without OAm–ITO NPs (Figure 2b).<sup>[88]</sup>

Similarly, the areal capacitance of MnO NP-based pseudocapacitor electrodes could be significantly increased by the insertion of OAm–ITO NPs using the abovementioned LE-LbL assembly method (Figure 2e).<sup>[91]</sup> In this case, the charge transfer resistance ( $R_{ct}$ , a semicircle in the middle-frequency region) and ion diffusion behavior (Warburg line in the low-frequency region) of the OAm–ITO NP-inserted electrode were significantly improved compared to the electrodes without OAm–ITO NPs (Figure 2f). That is, the periodic deposition of conductive ITO NP layers into a functional TMO NP (i.e.,  $\text{WO}_{2.72}$  or  $\text{MnO}_2$ ) film through a ligand exchange reaction notably reduced the internal resistance of the

electrodes, resulting in improved electrochemical performance. As a result, the design of efficient electrodes by combining functional NP (i.e., metal and TMO NP) assembly approaches with ligand engineering is a new breakthrough for increasing the performance of electrochemical electrodes for energy storage that can address the trade-off relationship between energy and power.

## 2.2. Ligand Exchange LbL Assembly for Increased Charge Transfer of Functional NP-Based Nanocomposites

Based on the significant influence of surface ligands on the electrical and electrochemical properties of functional NP-based nanocomposites, many research groups have reported a variety

of approaches to remove residual organic ligands bound to the surface of NPs or decrease the interdistance between adjacent NPs. However, in most cases, these approaches require additional treatments such as thermal annealing,<sup>[92]</sup> the use of chemical agents,<sup>[93]</sup> and the use of a mechanical press<sup>[94]</sup> after NP deposition onto the substrate, which may be difficult to directly apply to substrates such as heat/chemical agent-damageable textiles or mechanically vulnerable glasses. Furthermore, considering that the mutual interactions between neighboring NPs as well as between the NP and substrate can act as an important parameter in ensuring electrical and electrochemical stability of NP-based electrodes for energy storage, it is difficult for conventional physical adsorption processes (i.e., dip coating, painting, Meyer rod coating, and dispensing-writing methods) to control interfacial interactions.

As an alternative, the LbL assembly process, which is a solution-processable, ultrathin film fabrication technique, has attracted considerable attention because it is based on the complementary interactions between two different components, irrespective of the substrate size and shape.<sup>[95–103]</sup> In most cases, this approach has been performed using electrostatic interactions between electrostatically charged active components (i.e., inorganic NPs, carbon-based materials, or electrochemically active polymers) and oppositely charged polymers such as polyelectrolytes in aqueous media. Despite the notable advantages of the LbL assembly method, the use of bulky and insulating polymer linkers significantly restricts charge transfer between active components.

Recently, Cho and co-workers reported novel types of LbL self-assembly for functional NPs based on the in situ ligand exchange reaction between the hydrophobic ligands of NP and amine (NH<sub>2</sub>)-functionalized organic linkers in organic media.<sup>[50–57,104]</sup> In this process, the high affinity of amine moieties to metal surfaces (via covalent bonds)<sup>[105–108]</sup> effectively induces the replacement of insulating hydrophobic ligands of NPs with hydrophilic incoming ligands (i.e., HN<sub>2</sub>-functionalized dendrimers), showing dramatic changes in the surface chemistry (Figure 3a). As the deposition time of the NH<sub>2</sub>-dendrimer layer increased, the characteristic peaks originating from the hydrophobic ligand (i.e., PA) gradually disappeared, and new peaks arising from the hydrophilic moiety –NH<sub>2</sub> were observed, indicating the complete removal of insulating ligands from the NPs.<sup>[50]</sup> The reaction is complete in almost half an hour, which is quite fast compared to other organosulfur-based ligand exchange reactions that require several hours.<sup>[109–111]</sup> Additionally, it is worth noting that the change in the outermost ligands from being hydrophobic to being hydrophilic leads to excellent electrolyte wettability (or ion accessibility) in electrochemical energy applications, which improves the energy density and efficiency under high rate operation.<sup>[112,113]</sup> Furthermore, when applying small molecules as incoming ligands, only one molecular layer exists between vertically and horizontally adjacent NPs after ligand exchange reactions, which is quite different from conventional electrostatic LbL assembly<sup>[95,101]</sup> and blending methods<sup>[114]</sup> with many residual insulating ligands in the nanocomposites (Figure 3b). This unique phenomenon not only provides a significant improvement in interfacial charge transfer kinetics due to the effective elimination of polymeric ligands as well as a reduction in the separation distance between neighboring NPs but also enables high structural stability in various media (or electrolytes)

and under mechanical deformation (Figure 3c,d). As shown in Figure 3c, the mass of NP-based nanocomposite films measured by a quartz crystal microbalance (QCM) remained almost unchanged with an immersion time of ≈4 h in various solvents. In addition, the electrical conductivity change ( $\sigma/\sigma_0$ ) of the LE-LbL-assembled NP film was negligible even after 10 000 bending cycles, which was in stark contrast to that of an electron beam evaporated electrode, indicating excellent structural stability (Figure 3d).<sup>[52]</sup> These results demonstrate that LE-LbL-assembled NP films are chemically and mechanically stable.

Increasing the packing density of functional NPs within a limited electrode volume is challenging in electrodes for energy storage<sup>[115–118]</sup> and other integrated nanostructures.<sup>[57,119–121]</sup> Generally, NP-based electrodes with a high mass density cannot be easily achieved by conventional electrode preparation methods such as doctor blading or electrostatic LbL assembly without additional treatments (e.g., the use of a mechanical press or thermal annealing) due to the low-density nature of polymeric (or carbonaceous) materials and electrostatic repulsive forces among NPs with the same charge.<sup>[94,101,122–124]</sup> On the other hand, it has been reported that in situ LE-LbL assembly can produce densely packed NP multilayers without any NP agglomeration or segregation because the reported approach does not use charged species and/or bulky polymer ligands in organic media. In this study, the as-assembled Ag NP multilayers exhibited a high packing density of ≈60% (in volume), obtained from QCM measurements based on the Sauerbrey equation,<sup>[125]</sup> which was much higher than that of nanocomposites prepared using the abovementioned conventional methods (<30% packing density or ≈1 g cm<sup>-3</sup> mass density).<sup>[123,126,127]</sup>

One of the most attractive advantages of LbL assembly is that the loading amount of functional NPs can be easily and precisely modulated by controlling the deposition number. This unique characteristic also implies that the output performance of NP-based electrodes, such as electrical conductivity, catalytic activity, and areal capacity, can be improved through consecutive deposition of NPs.<sup>[55,128–132]</sup> That is, by simply increasing the bilayer number (*n*), the thickness and mass of NP-based multilayers are regularly increased without significant NP agglomeration, which can be expanded up to a micrometer-scale thickness irrespective of substrate size and shape (Figure 3e).<sup>[104]</sup> The scalability of this approach is highly advantageous in achieving high volumetric and areal energy densities, which are considered valuable performance factors in practical and commercial energy storage systems.<sup>[133]</sup> Additionally, this approach can be easily applied to automatic spray or roll-to-roll LbL deposition processes,<sup>[134,135]</sup> enabling fast and large-scale fabrication of flexible or wearable energy electronics. Thus, the efficient combination of NP assembly and ligand engineering processes provides a good approach for the preparation of NP-based electrodes with increased charge transfer kinetics as well as high energy density.

### 3. Ligand-Engineering-Based Energy Storage

In electrochemical energy systems, given that most electrochemical reactions involving the uptake and release of active species mainly occur on the surfaces of active materials, the

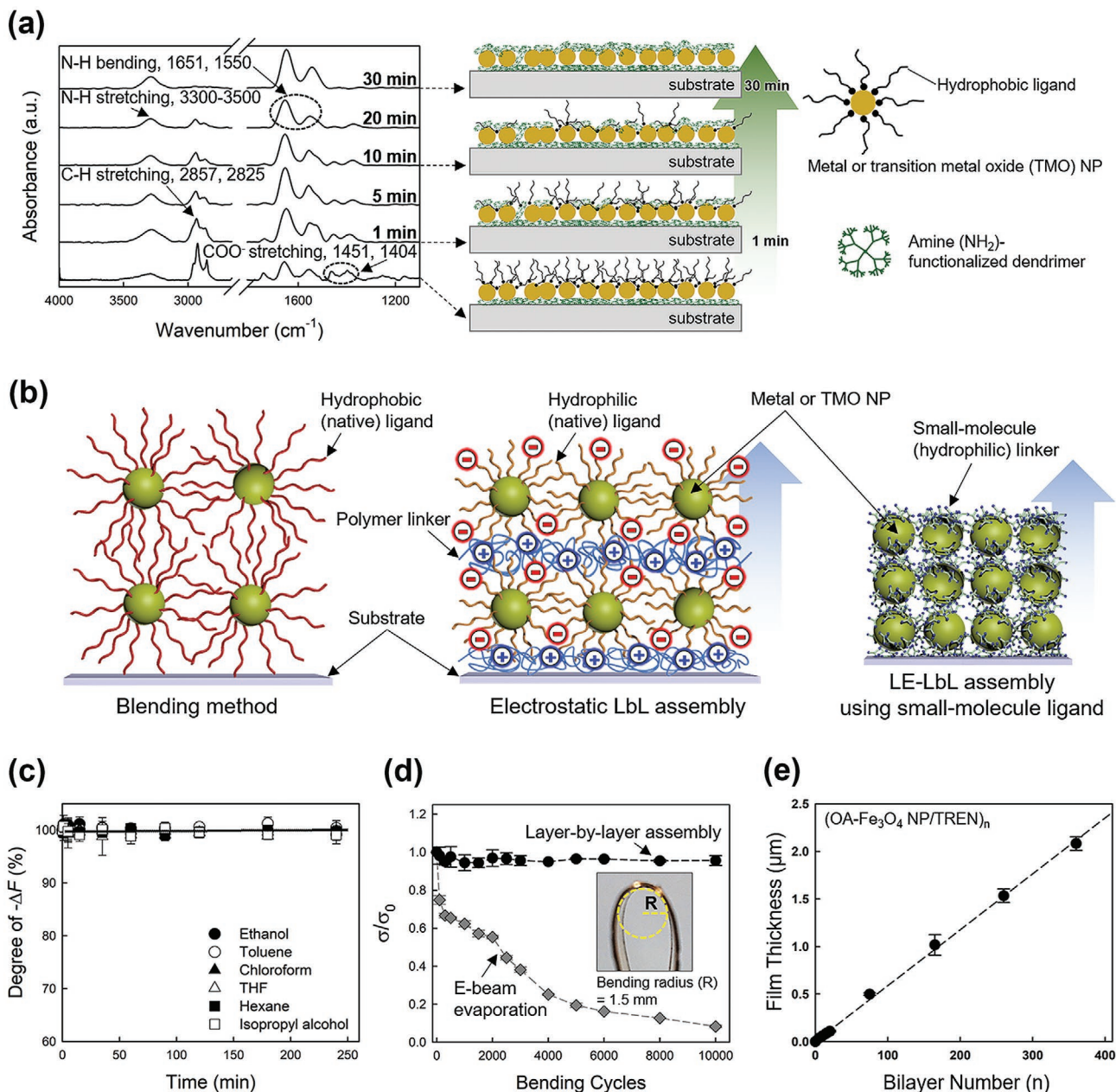


**Figure 3.** Nanoparticle (NP)-based nanocomposite film prepared by LE-LbL assembly. a) Fourier transform infrared (FTIR) spectra (left) and schematic representation (right) of LE-LbL-assembled PA-Ag NP/NH<sub>2</sub>-functionalized dendrimer multilayers as a function of the deposition time of the NH<sub>2</sub>-functionalized dendrimer. Adapted with permission.<sup>[50]</sup> Copyright 2013, American Chemical Society. b) Schematic diagram showing the structural differences of NP-based nanocomposites prepared by the conventional blending method (left), by electrostatic LbL assembly (middle), and by LE-LbL assembly using a small-molecule ligand (right). c) Mass change (-ΔF (%)) in LE-LbL-assembled multilayers in various organic solvents as a function of immersion time (min). Adapted with permission.<sup>[50]</sup> Copyright 2013, American Chemical Society. d) Electrical conductivity (σ/σ<sub>0</sub>) of Au NP-based thin films on plastic substrates prepared by LE-LbL assembly and electron beam evaporation. Adapted under the terms of the CC-BY Creative Commons Attribution 4.0 International license (<https://creativecommons.org/licenses/by/4.0>).<sup>[52]</sup> Copyright 2017, The Authors, published by Springer Nature. e) Film thickness of (OA-Fe<sub>3</sub>O<sub>4</sub> NP/small-molecule linker (TREN))<sub>n</sub> multilayers as a function of bilayer number (n). Adapted with permission.<sup>[104]</sup> Copyright 2018, Wiley-VCH.

proper modulation of the electrode interface chemistry is a decisive factor in the performance output. Further, the use of NP-based electrodes with an extremely large surface area significantly increases the number of electrochemical reactions per unit area.<sup>[6,15,136–138]</sup> In this section, these issues are discussed considering specific energy storage applications, such as lithium-ion batteries and electrochemical capacitors.

### 3.1. Lithium-Ion Battery: Size Effect of Energy Nanomaterials

Rechargeable batteries have been considered one of the most advanced energy storage systems to resolve the issues of fossil fuel depletion that have been constantly raised over past centuries. Since the lead–acid battery, the oldest rechargeable battery, was first invented in 1859,<sup>[139]</sup> tremendous research has

been devoted to exploiting suitable energy storage materials and electrode compositions that can meet the demands of high-performance electronics. Among the various metals for charge carriers in rechargeable battery systems, lithium (Li) is still the most promising charge carrier material due to its light weight, good ion mobility, lack of memory effect, and high energy density (reduction potential of  $-3.04$  V vs the standard electrode potential ( $E^0$ )<sup>[4,140]</sup>), and it has been widely applied to batteries (i.e., lithium-ion batteries, LIBs) for various commercial applications, such as medical devices, mobile electronics, and electric vehicles.<sup>[1,141,142]</sup> Furthermore, many challenging attempts are being made to design appropriate electrode structures to increase the energy and power density through advanced nanotechnologies involving surface ligand modulations of high-energy TMO NPs.

The energy density of battery systems basically depends on the intrinsic electrochemical nature of the active materials. Therefore, the development of high-voltage cathode and high-capacity anode materials and the full realization of their properties in battery cells are the prime routes for achieving batteries with high energy density (i.e., capacity  $\times$  voltage).

Since the first commercialization of bulk LiCoO<sub>2</sub>/C electrode-based rechargeable LIBs,<sup>[143]</sup> the low reversible capacity and low rate performance, which are closely related to the ion/electron diffusion kinetics, have steadily emerged as difficult and troublesome problems to overcome.<sup>[144]</sup> Accordingly, crystalline energetic NPs instead of bulk energetic materials have received attention as an alternative to solve the abovementioned issues. Specifically, the use of energetic NPs in battery electrodes not only provides an extremely large surface area that can increase the Faradaic reaction at a given sweep rate but also allows the fabrication of electrodes with well-defined nanostructures that promote ion diffusion within the lattices.<sup>[26,145–148]</sup> As a result, these phenomena contribute to the increase in capacity and electrochemical reactivity. Particularly, given that the ion diffusion time ( $t$ ) decreases as the charge/discharge sweep rate increases (Equation (1)), the effective specific capacity depends on the particle volume ratio with the following relationship<sup>[146]</sup>

$$\left[ r^3 - (r - L) \right]^3 / r^3 \quad (2)$$

where  $r$  and  $L$  represent the particle radius and ion diffusion length, respectively.

Therefore, to obtain the maximum specific capacity, the ion diffusion length should be greater than the particle radius. For example, if the charge/discharge cycle time of LiFePO<sub>4</sub> materials with a diffusion coefficient of  $10^{-14}$  D<sub>Li</sub> cm<sup>2</sup> s<sup>-1</sup> is 1 min,<sup>[149]</sup> their size should be smaller than 15 nm. These results suggest that a notable decrease in the ion diffusion pathway can be realized in nanoscale energy materials.

Ceder and co-workers also reported that the ion diffusion coefficient in LIB cells could be controlled according to the particle size.<sup>[29]</sup> In the case of bulk LiFePO<sub>4</sub> crystals as a cathode material, the diffusion of Li ions through 1D channels (i.e., (010) or (001) plane directions) is blocked or decelerated by Fe ions that occupy the channels (i.e., point defects), resulting in poor rate capability and high potential polarization (Figure 4a). On the other hand, particle size reduction to the nanometer scale significantly diminishes the defects that prevent the migration of

Li ions in lattices, allowing efficient utilization of Li ions under high rate operation (Figure 4d). That is, the reduced particle size increases the ion diffusion coefficient of LiFePO<sub>4</sub> cathode materials. Additionally, the expanded lattice spacing caused by nanosized particles aids in ion movement, which induces capacitive behavior at the interfaces with a higher rate capability than that of bulk electrodes for energy storage (Figure 4c,d).<sup>[150]</sup> Similarly, as the LiCoO<sub>2</sub> crystallite size decreases, a capacitive behavior with a disappearing plateau becomes dominant (Figure 4c), indicating the facile intercalation of Li ions into the surface layers with an enlarged interspacing distance (Figure 4d).

The nanosize effect of energy materials on electrochemical performance can also be observed in conversion-reaction-based anode materials. Tarascon and co-workers reported that crystalline  $\alpha$ -Fe<sub>2</sub>O<sub>3</sub> (hematite) NPs could store a larger amount of Li ions (i.e.,  $\approx 1$  Li per  $\alpha$ -Fe<sub>2</sub>O<sub>3</sub> or  $\alpha$ -Li<sub>1.0</sub>Fe<sub>2</sub>O<sub>3</sub>) than bulk iron oxide materials (i.e.,  $\approx 0.05$  Li per Fe<sub>2</sub>O<sub>3bulk</sub> or Li<sub>0.05</sub>Fe<sub>2</sub>O<sub>3bulk</sub>), and the NPs could more easily accommodate structural deformations than bulk NPs under Li intercalation.<sup>[151]</sup> These unique advantages of NPs strongly support the fact that  $\alpha$ -Fe<sub>2</sub>O<sub>3</sub> NP-based electrodes exhibit better cycle retention and capacity than bulk iron oxide-based electrodes. In addition, decreasing the size of energetic NPs further facilitates ion intercalation/deintercalation behavior into the crystal lattices.<sup>[152]</sup> Figure 4e shows the impedance spectra of anatase TiO<sub>2</sub> NP-based anode electrodes with various NP sizes ranging from 8.6 to 24.1 nm. In this case, the  $R_{ct}$  value analyzed from the radius of the semicircle in the low-frequency region gradually decreased from  $\approx 24.5$  to  $\approx 65$   $\Omega$  as the NP size decreased, indicating improved Li ion transfer kinetics at the electrode/electrolyte interfaces. As a result, the anode electrode with a smaller TiO<sub>2</sub> NP size showed much better electrochemical performance than the large-sized NP-based electrode at the same current density, demonstrating high rate performance (Figure 4f).

Although nanoscale energy materials have a beneficial effect on electrochemical performance, most studies on the nanosize effects of energy materials on electrochemical output have been analyzed without full consideration of bulky insulating organic ligands bound to the surface of energetic nanomaterials. As mentioned earlier, most energetic NPs, such as TMO NPs, have poor electrical conductivity, and the presence of organic ligands has synergistically fatal impacts on the charge transfer kinetics at the interfaces between neighboring NPs as well as between NPs and conductive supports. From this perspective, many studies on the preparation of TMO NP-based electrodes for energy storage have obvious limitations in solving a variety of performance issues, including the energy efficiency and cycle stability of LIB electrode assemblies.<sup>[153–155]</sup> Therefore, it is desirable that interface factors such as complementary interactions, structural design, and organic ligands should be considered for preparing NP-based LIB electrodes with high charge transport behavior; furthermore, these factors should be easily but finely controlled during electrode preparation.

### 3.2. Surface Modification of Energy NPs

Although a decrease in the size of energy materials can significantly improve ion diffusion kinetics in LIB electrodes, the



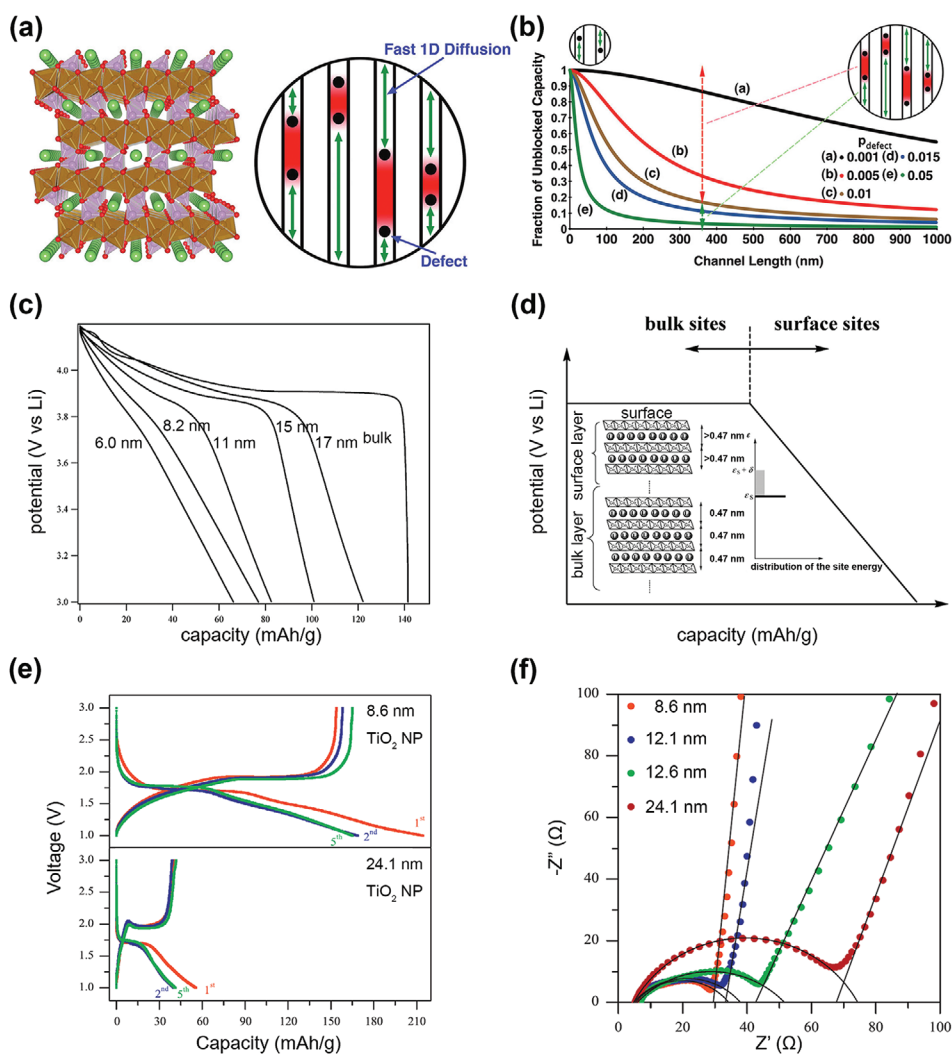


**Figure 4.** Electrochemical behavior of the NP-based LIB electrode. a) Representative crystal structure of  $\text{LiFePO}_4$  showing 1D channels for Li ion diffusion (left). Schematic illustration of Li ion diffusion behavior with point defects (right). b) Fraction of unblocked capacity versus channel length of  $\text{LiFePO}_4$  nanocrystals with different defect concentrations ( $\rho_{\text{defect}}$ ). In this case, the defect concentration decreases as the nanocrystal size decreases. a,b) Adapted with permission.<sup>[29]</sup> Copyright 2010, American Chemical Society. c) Discharge curves of  $\text{LiCoO}_2$ -based LIB cathodes with various crystallite sizes. d) Expected discharge behavior of nanosized  $\text{LiCoO}_2$ . The inset illustrates the representative crystal structure of  $\text{LiCoO}_2$  NPs with different interspacing values for the surface and bulk phases. c,d) Adapted with permission.<sup>[150]</sup> Copyright 2010, American Chemical Society. e) Electrochemical impedance spectra of  $\text{TiO}_2$ -based LIB anode electrodes with different particle sizes. f) Galvanostatic charge/discharge profiles for the first, second, and fifth cycles at a current density of  $20 \text{ mA g}^{-1}$  of  $\text{TiO}_2$  NP-based LIB anode electrodes with different particle sizes (8.6 and 24.1 nm). e,f) Adapted with permission.<sup>[152]</sup> Copyright 2013, Elsevier.

use of the energy NPs still has much difficulty in sufficiently enhancing LIB performance due to their poor electrical conductivity. To overcome this problem, the surface of energy materials using conductive materials such as conducting polymer, carbon, and metal NPs has been modified through the wrapping or coating of conductive materials such as conducting polymer, carbon, and metal NPs.<sup>[156–161]</sup> Generally, the coating of carbon materials on the surface of the energy NPs creates a conductive thin layer, forming a core-shell structures. Furthermore, it should be noted that the conductive carbon shells also serve as a buffer layer against periodic volume change of energy NPs. For example, Passerini and co-workers reported the carbon-coated  $\text{ZnFe}_2\text{O}_4$  NPs for carboxymethylcellulose (CMC)-based

aqueous LIB anodes.<sup>[159]</sup> A few nanometer-thick carbon layer-coated  $\text{ZnFe}_2\text{O}_4$  NPs could form the well-connected electrical percolation network within the resulting NP-based nanocomposite electrode (Figure 5a), resulting in the more improved rate-performance and capacity reversibility compared to bare NP-based electrode made of CMC or PVDF-HEP (Figure 5b). Additionally, they demonstrated that the carbon shell prevented the direct contact between the energy NPs and the electrolyte, which could resultantly restrict the formation of an unstable amorphous polymeric layer (i.e., solid electrolyte interface (SEI) layer) by continuous electrolyte decomposition reaction.<sup>[162]</sup>

As another approach, various metal NPs have been anchored on the surface of energy materials. Stevenson and co-workers

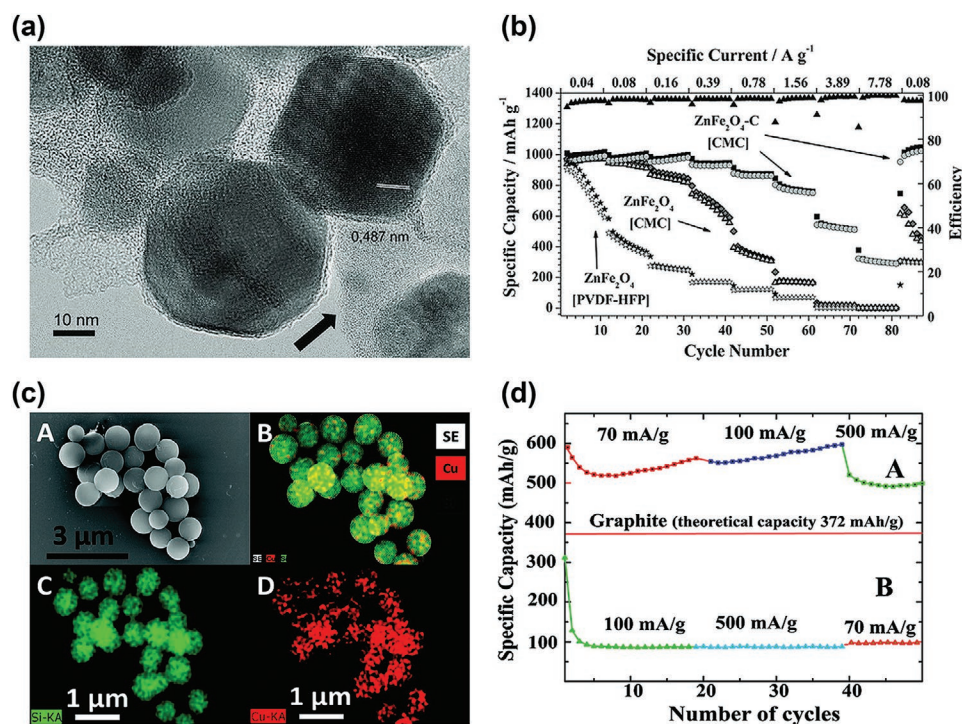


**Figure 5.** Surface modification of energy material. a) High-resolution transmission electron microscopy (HR TEM) image of carbon-coated  $\text{ZnFe}_2\text{O}_4$  ( $\text{ZnFe}_2\text{O}_4\text{-C}$ ) NPs. The carbon thin layer is uniformly covered on the  $\text{ZnFe}_2\text{O}_4$  NP surface. In this case, an additional carbon layer (black arrow) around the  $\text{ZnFe}_2\text{O}_4\text{-C}$  NPs connects adjacent NPs and forms a continuous conducting network. b) Electrochemical properties of  $\text{ZnFe}_2\text{O}_4\text{-C}$  NP-based LIBs monitored by the galvanostatic charge/discharge processes. a, b) Adapted with permission.<sup>[159]</sup> Copyright 2012, Wiley-VCH. c) Scanning transmission electron microscopy (STEM) image of Cu NP-coated large-sized Si NPs (A) and corresponding elemental mapping images (B–D) collected using energy-dispersive X-ray spectroscopy (EDS). d) Cycle-number-dependent specific capacity for Si NP-based LIBs with (A) and without (B) Cu NP at different current density of 70, 100, and 500  $\text{mA g}^{-1}$ , respectively. The red line in the middle region indicates the specific capacity of a commercial graphite-based cell. c, d) Adapted with permission.<sup>[161]</sup> Copyright 2012, American Chemical Society.

reported the copper (Cu)-coated amorphous silicon (Si) particles prepared by low temperature polyol reduction process.<sup>[161]</sup> As shown in Figure 5c, the uniformly coated Cu NPs on the surface of large-sized Si NPs could play a role as a conductive relay, allowing the improved charge transfer kinetics at the interface between neighboring NPs. The Li-ion half-cell based on the Cu-decorated Si particle showed much better energy efficiency (i.e., specific capacity and cycle retention) than the bare Si particle-based one (Figure 5d). These results implied that the incorporated Cu not only reduced the internal resistance of the electrode, but also suppressed the undesired solvent decomposition at the electrode/electrolyte interface. In addition to Cu NP, various metal NPs such as Sn,<sup>[79]</sup> Ag,<sup>[163]</sup> and Au<sup>[164]</sup> have been also employed to improve the electrical conductivity and energy efficiency of LIB electrodes.

These previous reports clearly demonstrate that improving the electrical conductivity at the numerous interfaces of energy NPs within LIB electrode is of great importance for achieving high electrochemical reactivity and operation stability. However, it should be noted that the quality of such incoming conductive species is highly dependent on the complex synthesis conditions (e.g., temperature, reaction time, and molar concentration of active species), and the electrode formation is largely limited to convention blending technique with unfavorable interfacial interactions between the respective active components. Therefore, to maximize energy efficiency, the integrated and

systematic electrode design for active nanomaterials and their nanocomposites should be carefully considered.

### 3.3. Interfacial Ligand Design for Improved Charge Transport of NP-Based LIB Electrodes

As a common approach to improve the charge transport kinetics, various carbon materials as conductive enhancers have been actively combined with poorly conductive TMO materials through physical mixing with or without insulating polymer binders.<sup>[22,165,166]</sup> However, the low mass density of the inserted TMO within the electrode and the insulating nature of polymer binders limit the achievement of high areal and volumetric capacities, particularly at high sweep rates. In this respect, if metal NPs can be used as conductive enhancers in TMO NP-based electrodes without the aid of additional polymer binders, this approach may be a breakthrough to resolve the low mass density of TMO materials and the low charge transfer kinetics of conventional electrodes.<sup>[167]</sup> Furthermore, a highly uniform combination of high-quality TMO NPs and metal NPs through ligand engineering can be an effective way to synergistically affect the electrochemical performance of LIB electrodes with high charge transfer efficiency.

These possibilities were systematically demonstrated by the ligand-engineering- (or ligand exchange reaction)-induced LbL assembly of hydrophobic  $\text{Fe}_3\text{O}_4$  NPs (i.e., stabilized by

OA) with consecutive insertion of metal (platinum, Pt) NPs using flash sputtering processes (Figure 6a).<sup>[104]</sup> In this case, the bulky OA ligands of Fe<sub>3</sub>O<sub>4</sub> NPs were effectively replaced by NH<sub>2</sub>-functionalized small organic ligands (i.e., tris(2-aminoethyl)amine, TREN)) during LE-LbL assembly in organic media. This approach allowed dense packing of Fe<sub>3</sub>O<sub>4</sub> NPs in the formed Fe<sub>3</sub>O<sub>4</sub> NP/TREN multilayers (mass density of ≈3.5 vs ≈5.2 g cm<sup>-3</sup> for the bulk) because of the absence of electrostatic repulsion between neighboring Fe<sub>3</sub>O<sub>4</sub> NPs as well as insulating polymer binders, indicating a significant reduction in interparticle distance that can facilitate electron transport between adjacent NPs. In addition, the formed multilayer films generate a number of nanopores that can create an effective

ion (i.e., electrolyte) path, which is a critical factor to achieve high rate capacity in densely packed electrodes.<sup>[167–173]</sup> After the LE-LbL deposition of Fe<sub>3</sub>O<sub>4</sub> NPs, the Pt NPs were periodically introduced into the Fe<sub>3</sub>O<sub>4</sub> NP/TREN multilayers via sputtering methods under optimized conditions (i.e., current and time), resulting in the uniform distribution of Pt NPs within the multilayer films without any notable morphological changes, as shown in field-emission scanning electron microscopy (FE-SEM) and energy-dispersive spectrometry (EDS) mapping images (Figure 6b). Importantly, the inserted Pt NPs form stable covalent bonds with the NH<sub>2</sub> moieties of small-molecule linkers, preventing undesired molecule dissolution in the continuous charge/discharge processes.

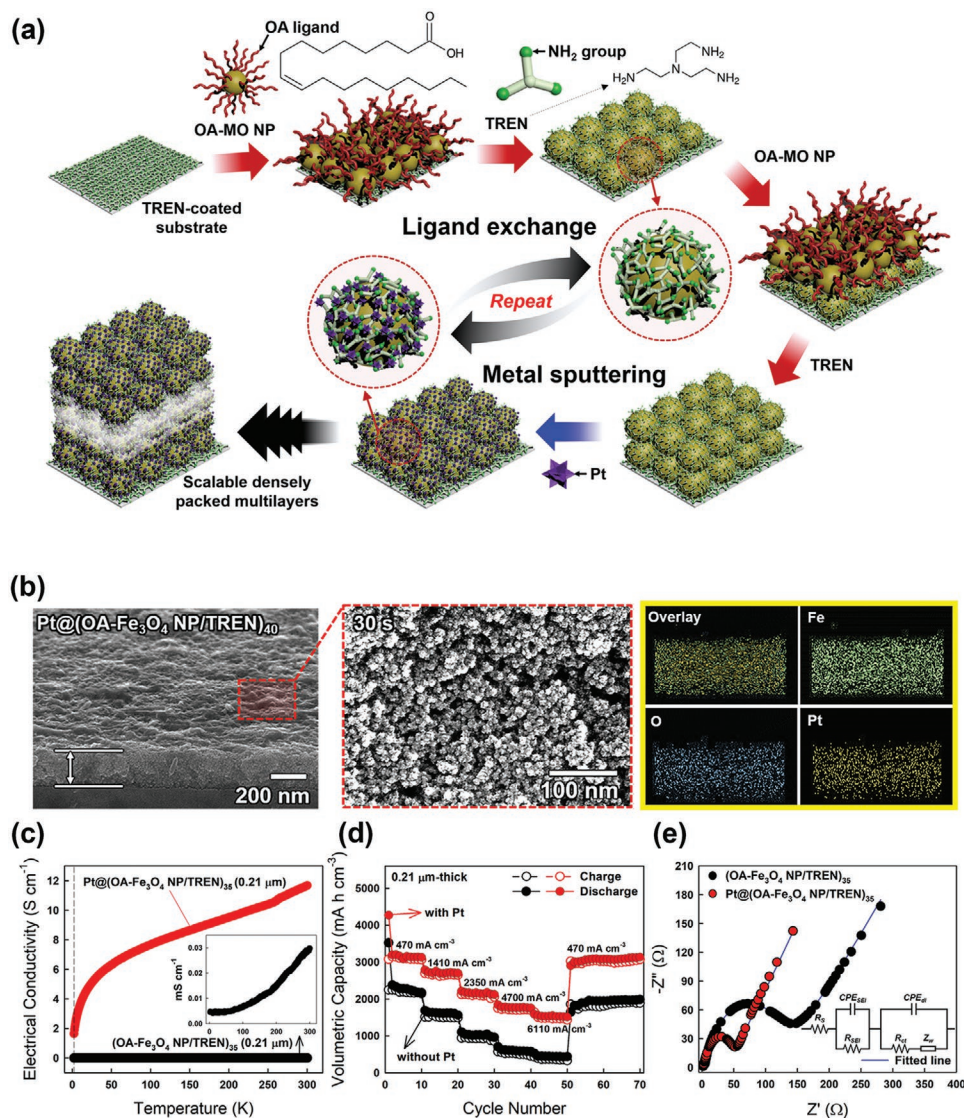


**Figure 6.** LE-LbL-assembled LIB anode. a) Schematic illustration of the preparation of Fe<sub>3</sub>O<sub>4</sub> NP-based anode electrodes through metal sputtering combined with LE-LbL assembly. b) FE-SEM (left and middle) and EDS mapping images of metal NP-inserted Fe<sub>3</sub>O<sub>4</sub> NP/TREN anode electrodes. The planar FE-SEM image indicates the surface of the electrode (red dotted box), and the EDS mapping represents the cross section of the electrode (yellow solid box). c) Temperature (*K*)-dependent electrical conductivity of Fe<sub>3</sub>O<sub>4</sub>/TREN electrodes with (red line) or without (black line) Pt sputtering. The inset indicates enlarged Fe<sub>3</sub>O<sub>4</sub>/TREN without Pt NPs. d) Volumetric capacity of each electrode at various current densities ranging from 470 to 6110 mA cm<sup>-2</sup>. e) Electrochemical impedance spectra of (OA-Fe<sub>3</sub>O<sub>4</sub> NP/TREN)<sub>35</sub> and Pt@(OA-Fe<sub>3</sub>O<sub>4</sub> NP/TREN)<sub>35</sub> electrodes. The inset indicates the representative equivalent circuit. a–e) Adapted with permission.<sup>[104]</sup> Copyright 2018, Wiley-VCH.

In general, bulk magnetite exhibits good electrical conductivity ( $\approx 10^2 \text{ S cm}^{-1}$ )<sup>[174]</sup> compared to other crystalline TMOs. However, as mentioned above, numerous insulating ligands surrounding the materials as well as the nanosize effect of  $\text{Fe}_3\text{O}_4$  NPs significantly hinder electron transport between neighboring NPs, resulting in a lower electrical conductivity. The LE-LbL assembly of  $\text{Fe}_3\text{O}_4$  NP/TREN films clearly demonstrated the effect of native organic ligands on the electrical properties (Figure 6c). The formed multilayer films exhibited an increased electrical conductivity of  $\approx 2.8 \times 10^{-5} \text{ S cm}^{-1}$  in contrast to the insulating characteristics of drop-cast OA- $\text{Fe}_3\text{O}_4$  NP films, which further increased up to  $\approx 11.6 \text{ S cm}^{-1}$  after metal sputtering.

As a result, the Pt NP-incorporated  $\text{Fe}_3\text{O}_4$  NP/TREN films (Pt@( $\text{Fe}_3\text{O}_4$  NP/TREN)) showed excellent volumetric capacity ( $\approx 3195 \text{ mA h cm}^{-3}$  at  $470 \text{ mA cm}^{-3}$ ) and rate performance with superior cycle retention compared to multilayers without metal sputtering (Figure 6d), indicating that the combination of LE-LbL assembly and sputtered metal NPs can noticeably reduce the internal resistance originating from bulky ligands and the semiconducting nature of TMO NPs (Figure 6e). In particular, the periodic insertion of Pt NPs by sputtering into the LE-LbL-assembled ( $\text{Fe}_3\text{O}_4$  NP/TREN)<sub>n</sub> films additionally decreases the  $R_{\text{ct}}$  of the electrodes from 143.5 to 52.1  $\Omega$  due to the enhanced electron transfer. Surprisingly, the formed electrodes showed a specific capacity of  $\approx 913 \text{ mA h g}^{-1}$  (>98% of the theoretical capacity of  $\text{Fe}_3\text{O}_4$ ) despite the high mass density, suggesting that ligand exchange with hydrophilic small organic compounds provides efficient utilization of the active materials and good electrolyte wettability. Although the electrodes without metal sputtering have shown low output performance compared to metal NP-inserted electrodes, it is worth noting that, despite the absence of additional conductive enhancers, the volumetric capacity obtained ( $\approx 2305 \text{ mA h cm}^{-3}$ ) is much better than that of physically blended TMO material-based electrodes containing a number of bulky organic compounds, such as polymer binder and OA ligands.<sup>[175–180]</sup> Furthermore, these results clearly demonstrate that the efficient removal of bulky ligands through LE-LbL assembly is highly beneficial for the interface charge transport of TMO NP-based LIB electrodes, thus enabling good energy efficiency and cycle retention.

### 3.4. Electrochemical Capacitors: Ligand-Engineering-Based Current Collector Design for Efficient Charge Transport

In contrast to batteries with a high energy density resulting from diffusion-controlled Faradaic reactions in the bulk phase, electrochemical capacitors (or supercapacitors), including electric double layer capacitors (EDLCs) and pseudocapacitors, exhibit higher power capability and a long cycle life due to the fast charge storage reactions on/near the surface of active materials that do not involve notable crystallographic phase changes.<sup>[2,181]</sup> In particular, pseudocapacitive materials with battery-like redox behaviors (e.g., hydrous  $\text{RuO}_2$ ,  $\text{MnO}_2$ ,  $\text{Co}_3\text{O}_4$ ,  $\text{Fe}_3\text{O}_4$ , and mixed transition metal oxides) have received attention over the past decade because they can deliver much higher energy density at high sweep rates than EDLC materials (i.e., carbonaceous

materials).<sup>[182,183]</sup> Although there is some confusion in clearly distinguishing the difference between battery and pseudocapacitive materials due to the improved rate performance of nanomaterial-based battery systems (see Section 3.1.), the electrochemical behavior of pseudocapacitive materials is not significantly limited by slow solid-state ion diffusion kinetics at various scan rates.<sup>[14,25,182]</sup> Therefore, interface control and the design of energetic NPs are critical for pseudocapacitive reactions that occur at the surface of electrodes at a depth of several nanometers. In the same direction, the interfacial resistance between the NP and the current collector also affects the electrochemical output.

The contact resistance arising from the NP/NP and NP/current collector interfaces is highly associated with sluggish electron and ion transport of pseudocapacitor electrodes. Zheng reported that the contact resistance between the current collector and active materials is the dominant factor in the total internal resistance of electrochemical capacitor systems, thus significantly influencing output performance.<sup>[184]</sup> Therefore, the current collector requires high electrical conductivity and adequate surface conditions, enabling the stable adsorption of active materials.

In recent studies, highly porous fabrics (e.g., carbon cloth, carbon felt, or textiles) with extremely large surface areas have been intensively used as current collectors or substrates capable of depositing various energy materials and/or conductive enhancers.<sup>[52,185–189]</sup> These fabric-based current collectors allow a substantial increase in the mass loading of pseudocapacitive NPs per unit area compared to nonporous flat substrates, resulting in the efficient utilization of active materials during fast charge/discharge cycles for a high-performance wearable energy supplier.<sup>[187,190]</sup> However, to this end, fabrics with insulating properties should be preferentially converted to conductive fabrics while maintaining their mechanical properties. For example, it was reported that Au NPs were densely deposited onto textile substrates through LE-LbL assembly with small-molecule linkers in organic media, forming highly porous metallic textiles with exceptional mechanical stabilities (Figure 7a,b).<sup>[52,191]</sup> These studies systematically demonstrated that the efficient removal of hydrophobic insulating ligands bound to Au NPs and the consequent reduction in interparticle distance could achieve metal-like conductivity ( $\approx 10^5 \text{ S cm}^{-1}$ ) while preserving their mechanical and geometrical characteristics. The resulting electrical properties of metallic textiles as current collectors are superior to those of carbon material-coated materials and conventional electrostatic LbL-assembled Au NP films.<sup>[94,192]</sup> This replacement of bulky ligands by small-molecule linkers greatly reduces the interfacial resistance between active materials such as pseudocapacitive NPs and current collectors, thus improving the rate performance.<sup>[184,193]</sup>

The potential applicability of metallic textiles as a current collector for pseudocapacitors was demonstrated by the successive LE-LbL deposition of TMO NPs (i.e.,  $\text{Fe}_3\text{O}_4$  and  $\text{MnO}_2$  NPs for negative and positive pseudocapacitive materials) on prepared metallic textiles. In this case, the bulky insulating ligands (i.e., OA ligands) of TMO NPs were also exchanged with hydrophilic small-molecule linkers, forming densely packed TMO NP arrays with improved charge transport. In stark contrast

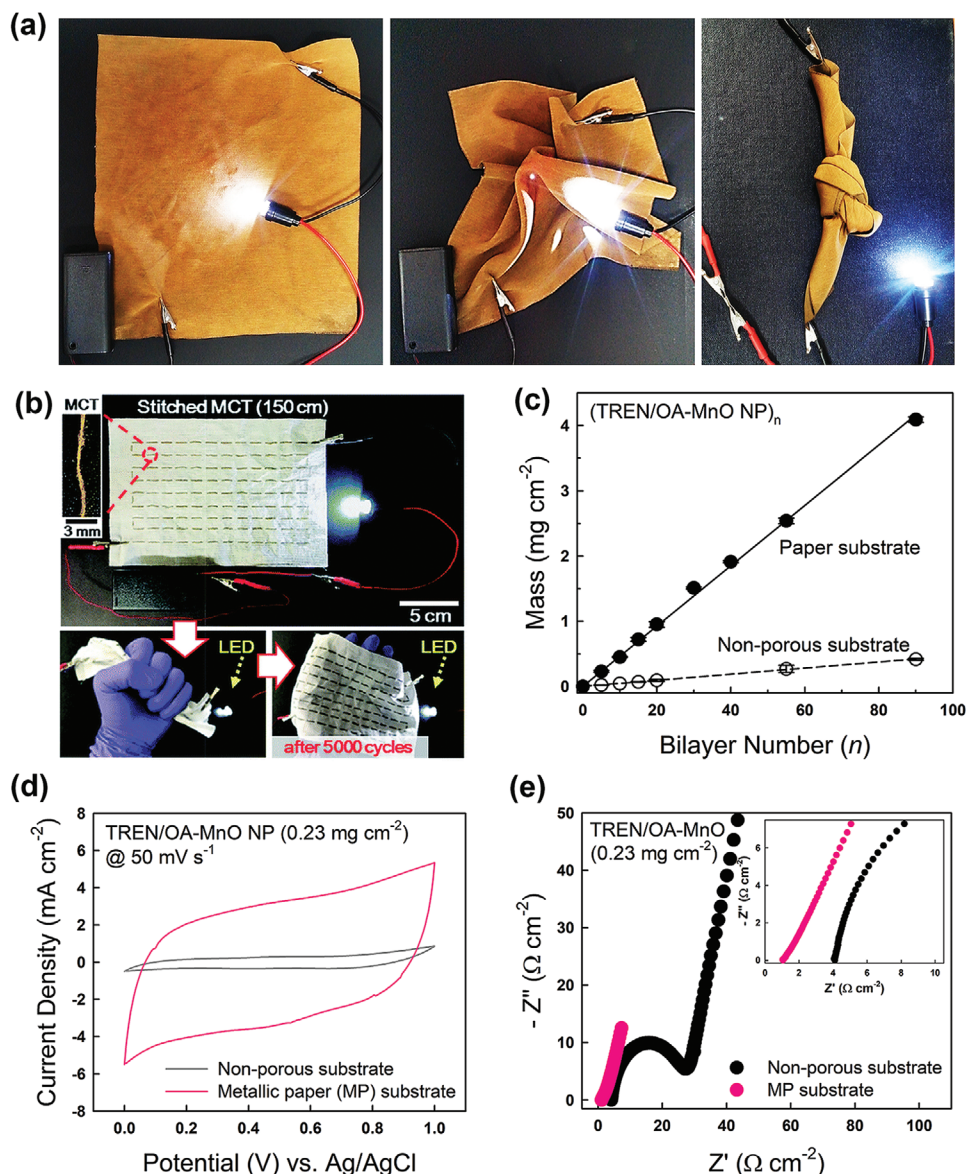


**Figure 7.** Textile-based current collector for improved charge transfer kinetics. a,b) Photographs of metallic textiles (a) and threads (b) connected to LED bulbs under various mechanical deformations. In this case, the metallic fabrics were prepared by coating with Au NP/TREN multilayers. c) Bilayer-number-dependent loading amount ( $\text{mg cm}^{-2}$ ) of MnO NPs onto porous (paper) and nonporous (flat) substrates. d) CVs and e) electrochemical impedance spectra of porous and nonporous substrate-based electrodes. The inset of (e) indicates the enlarged spectra in the high-frequency region. a,c–e) Adapted under the terms of the CC-BY Creative Commons Attribution 4.0 International license (<https://creativecommons.org/licenses/by/4.0/>).<sup>[52]</sup> Copyright 2017, The Authors, published by Springer Nature. b) Adapted with permission.<sup>[191]</sup> Copyright 2018, The Royal Society of Chemistry.

to nonporous flat substrates, metallic textiles accommodate a much greater number of TMO NPs per unit area, enabling high areal capacitance (Figure 7c). As a result, despite the same deposition numbers, the metallic textile-based supercapacitor electrodes exhibited approximately 10 times higher areal performance and lower internal resistance than flat substrate-based electrodes (Figure 7d,e), showing improved charge transfer kinetics at the interface of the TMO NP multilayer/current collector. It is worth noting that the extremely increased surface area of the textile-based electrode allows much thinner active layer than that of nonporous flat substrate-based one at the same loading amount of active materials. As a result, metallic

textile-based electrodes showed a significantly reduced  $R_{ct}$  value of  $0.08 \Omega \text{ cm}^{-2}$  compared to the nonporous electrode ( $R_{ct} \approx 23.4 \Omega \text{ cm}^{-2}$ ), demonstrating that the charge transport length was decreased by highly porous structures (Figure 7e).

### 3.5. Modification of Electronic Structure of Pseudocapacitive Material

Chemical doping is an effective way that can improve the electrical property of pseudocapacitive materials.<sup>[194,195]</sup> That is, incorporation of dopants into crystalline materials

changes their electronic structure, thereby providing a better electrical conductivity and electrochemical performance in energy storage systems. Zhou and co-workers reported that the electrical conductivity of  $\alpha$ -MnO<sub>2</sub> microsphere could be significantly increased by Al<sup>3+</sup> ion doping, resulting in high specific capacitance and excellent cycling stability (91% of initial value after 15 000 cycles).<sup>[195]</sup> They also demonstrated that the electrochemical performance strongly depended on according to the reaction molar ratio between Al<sup>3+</sup> and Mn<sup>4+</sup> in the doping processes, and could show the better electrical property at higher dopant concentration.

Another approach for improving the electrical properties of pseudocapacitive materials is to control oxygen vacancy within the materials.<sup>[196,197]</sup> Dunn and co-workers investigated the effect of oxygen vacancies on the electrochemical characteristics of  $\alpha$ -MoO<sub>3-x</sub>.<sup>[197]</sup> In this case,  $\alpha$ -MoO<sub>3-x</sub> with oxygen vacancies exhibited higher capacity with fast charge transfer kinetic (i.e., capacitive behavior) compared to the fully oxidized one. They also demonstrated that the generated oxygen vacancies act as a shallow donor to increase the carrier concentration in the lattices, which resultantly improve the electrical conductivity of  $\alpha$ -MoO<sub>3-x</sub>.<sup>[198]</sup> However, despite the unique advantages of such chemical doping, the dopants should be carefully selected because the structural instability after doping can also lead to the performance fading during long-term cycling operations (more than several thousand cycles).<sup>[199,200]</sup>

### 3.6. LE-LbL Design for Scalable Areal Performance in Electrochemical Capacitor Application

Scalable areal performance is highly attractive for achieving high energy density in limited areas. However, at the same time, it is imperative to consider the optimized electrode structure for facile ion transport and high electrical conductivity because the loading mass per unit area of poorly conductive energy materials such as pseudocapacitive NPs is directly related to the areal capacitance. Recently, it was reported that the increased overall internal resistance of electrodes according to the increase in the mass loading of pseudocapacitive TMO NPs could be reduced through the periodic insertion of conductive NPs into LE-LbL-assembled pseudocapacitive NP multilayers (Figure 8a–d).<sup>[91,191]</sup> In this case, the surfaces of the inserted conductive NP layers (i.e., TOA-Au NPs or OAm-ITO NPs) were covalently bonded to the amine groups of small-molecule ligands via the same ligand exchange reaction as that used for the TMO NP layers and acted as an electron transport layer between vertically adjacent TMO layers (Figure 8a,c). In addition, the periodically inserted conductive NPs were uniformly distributed within the electrodes without NP agglomeration or segregation, suggesting the formation of efficient electron paths (Figure 8b,d). With the aid of conductive NP layers, the internal resistance of the overall electrode was notably decreased compared to that of electrodes without conductive NP layers, resulting in improved electrochemical performance (Figure 8e,f). As a result, the asymmetric solid-state cells consisting of conductive NP-inserted LE-LbL electrodes (i.e., OA-MnO NP-based positive electrodes and OA-Fe<sub>3</sub>O<sub>4</sub> NP-based negative electrodes) showed

much better energy and power densities than other fiber-based electrochemical capacitors as well as LE-LbL electrodes without a conductive NP layer, further demonstrating the optimized electrode structure for efficient charge transfer kinetics (Figure 8g).<sup>[201–208]</sup> These results demonstrate that the surface ligand-engineering-induced assembly approach can provide an important basis for designing high-energy NP-based electrodes with improved charge transport and scalable/stable energy storage compared with traditional electrodes.

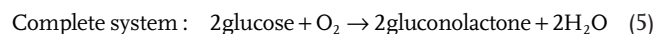
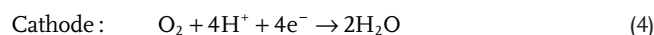
## 4. Ligand-Engineering-Based Energy Conversion

There has been considerable interest in various energy conversion devices. Among them, biofuel cells (BFC), which convert chemical energy into electrical energy, are considered portable and implantable energy sources.<sup>[209]</sup> Recently, several researches for improving the performance of BFC have focused on the increase of the active surface area of the electrode and/or the enhancement of electron transfer efficiency between the electrode surface and the enzyme. In this section, we review the recent progress of BFC electrodes composed of metal NPs and enzymes. We also discuss how the metal NP/enzyme multilayered electrodes based on LE-LbL assembly can increase the charge transfer efficiency, and furthermore enhance the BFC performance.

### 4.1. Concept of Biofuel Cells

Another attractive energy source is an enzymatic BFC, which allows the conversion of biochemical energy from humans, such as the conversion of glucose to electricity.<sup>[210,211]</sup> Although the power output of BFCs is much lower than that of other power sources, such as conventional fuel cells, BFCs have received much attention as a microscale power source for various biological and biomedical systems, including implantable devices, due to their high biocompatibility and operation under mild conditions (i.e., room temperature and near-neutral pH). Based on these notable advantages, many research efforts have been devoted to the development of BFCs with a higher power output than that of previous BFCs.<sup>[8,212,213]</sup>

Generally, enzymatic BFCs are composed of an anode coated by an enzyme layer (mainly glucose oxidase (GOx)) and a cathode coated by an ORR catalyst (e.g., bilirubin oxidase (BOD), laccase, Au NP, or Pt NP), which induces the following electrochemical reactions in an aqueous electrolyte solution containing glucose fuel.



Through these electrochemical reactions, effective electron transfer between the enzyme and electrode plays a significant role in determining the BFC performance. Therefore, a variety of strategies have been suggested for the fabrication

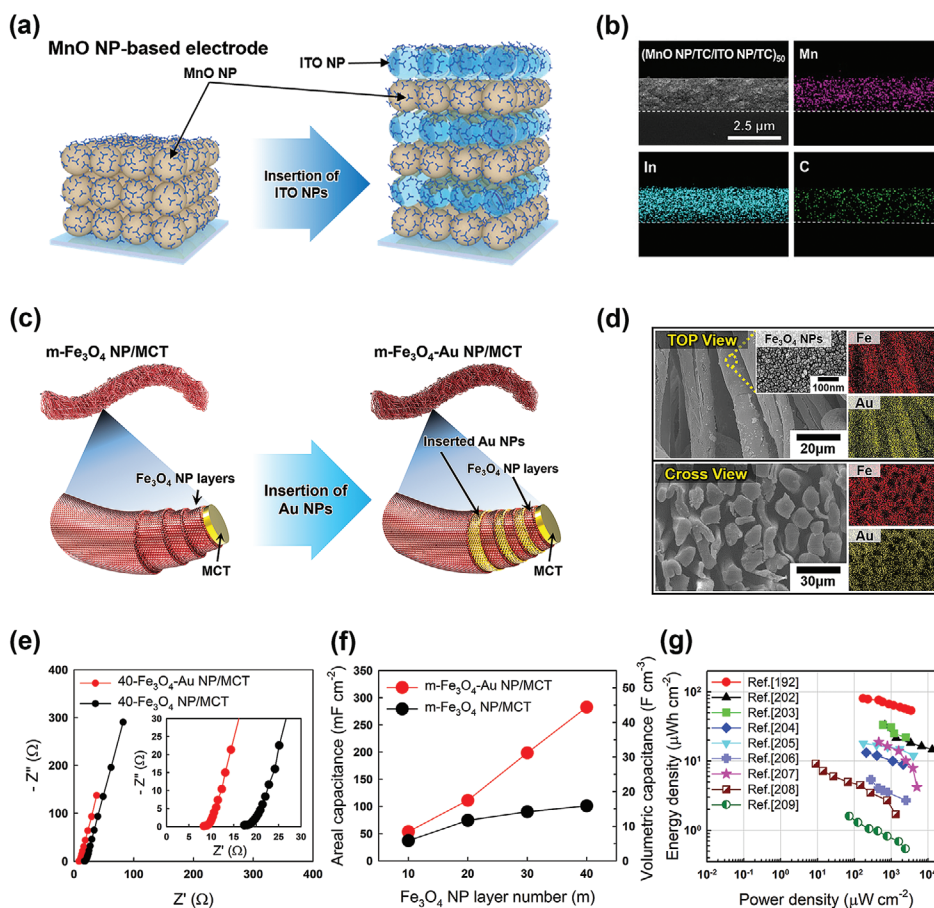


**Figure 8.** Scalable areal performance. a) Schematic illustration of the alternating deposition of pseudocapacitive MnO NPs and conducting ITO NPs through ligand-engineering-based LbL assembly. Adapted with permission.<sup>[91]</sup> Copyright 2019, American Chemical Society. b) Schematic illustration of the periodic insertion of the Au NP layer into Fe<sub>3</sub>O<sub>4</sub> NP-based multilayer negative electrodes. c) Electrochemical impedance spectra of 40-bilayer electrodes with or without the insertion of Au NP layers. d) Comparison of the areal and volumetric capacitance of the electrodes as a function of bilayer numbers. e) Ragone plots of the areal performance of the solid-state thread-type supercapacitor prepared by ligand-engineering-induced assembly. b–e) Adapted with permission.<sup>[91]</sup> Copyright 2018, The Royal Society of Chemistry.

of high-performance BFC electrodes over the last few decades, which are closely related to the strategies to enhance the electrical and electrochemical performance of BFCs through: 1) the use of carbon material-based supports (i.e., porous carbon, carbon nanotubes, and reduced graphene oxide (r-GO)) with large surface areas and high electrical conductivities (<300 S cm<sup>-1</sup>), 2) the use of redox mediators between the enzyme and the conductive support, and/or 3) the introduction of metal NPs into GOx. To the best of our knowledge, the highest power performance reported to date is a power output of 2.18 mW cm<sup>-2</sup> obtained from redox-mediated electron transfer-based BFCs (MET-BFCs).<sup>[214]</sup> On the other hand, it has been reported that conventional direct electron transfer-based BFCs (DET-BFCs) using a carbon material-based support without the use of redox mediators generally exhibit an extremely low power output of a few μW cm<sup>-2</sup>.<sup>[215]</sup> Despite the low performance of DET-BFCs, recent research trends have focused on the development of high-performance DET-BFCs that can overcome several critical issues of MET-BFCs, such as instability, toxicity, and the complex synthesis of redox mediators.

To improve the performance of DET-BFCs through effective charge transfer between the enzyme and electrode, the number of electrochemically inactive and insulating organic compounds existing within the electrodes of DET-BFCs should be minimized. Furthermore, it is desirable that the electrodes have higher electrical conductivity and a larger active surface area than those of conventional carbon material-based electrodes to enhance the charge transfer efficiency between the enzyme and electrode. As mentioned in previous sections, these requirements are directly applied to energy storage electrodes such as batteries and supercapacitors.

In this section, we describe conventional BFCs reported to date and then introduce a state-of-the-art DET-BFC using ligand engineering. Additionally, we suggest possibilities for maximizing the charge transfer efficiency of DET-BFCs through ligand-exchange-induced NP assembly. Furthermore, we describe how the interfacial design of electrodes and the ligand control of metal NPs can influence the charge transfer efficiency of DET-BFCs as well as the electrical/electrochemical properties of electrodes.

## 4.2. Carbon-Based Materials as a Host Electrode for Conventional BFCs

Carbon-based materials such as CNTs and/or r-GOs have been widely used to improve the electrical conductivity, active surface area, and mechanical properties of host electrodes. Mano and co-workers demonstrated that carbon materials such as carbon fibers and porous CNTs could be used as host electrodes for the preparation of GOx-coated anodes and BOD-coated cathodes. They also reported that the maximum power density ( $\approx 0.7 \text{ mW cm}^{-2}$ ) of CNT-based BFCs was four times higher than that of carbon fiber-based BFCs due to the facile mass (or ion) transfer by the porous structure of the CNT host electrode (Figure 9a,b).<sup>[216]</sup> Cosnier and co-workers also reported that disk-type CNT-enzyme composite electrodes, in which the disk was compressed by a hydraulic press, exhibited a maximum power density of  $1.3 \text{ mW cm}^{-2}$  under physiological conditions (Figure 9c,d).<sup>[217]</sup> Furthermore, considerable research efforts have focused on modifying the chemical and mechanical properties of carbon-based host electrodes to enhance power output and operational stability. However, the low electrical conductivity ( $< 300 \text{ S cm}^{-1}$ ) of carbon-based materials compared with that of bulk metal and the unfavorable interfacial interactions between hydrophobic carbon-based host electrodes and hydrophilic enzymes significantly increase the internal resistance

and simultaneously decrease the overall operational stability of BFC electrodes. Although surface modifications of carbon materials can induce a stable electrostatic adsorption of negatively charged enzymes (at pH 7.4) through the introduction of positively charged amine groups (i.e.,  $\text{NH}_3^+$  groups) onto the surface of carbon materials, this chemical modification greatly decreases the electrical conductivity of carbon materials. Therefore, if the next-generation host electrode for high-performance BFCs can achieve bulk metal-like conductivity and stable adsorption with enzymes that cannot be easily realized by conventional carbon-based materials, we believe that it can significantly contribute to the preparation of high-performance BFCs with enhanced electrical communication between the electrode and enzymes as well as operational stability.

## 4.3. Redox Mediators between the Enzyme and Conductive Support for MET-BFCs

One of the most widely used approaches for improving the power output of BFCs is the use of redox mediators acting as an electron transfer bridge between the enzyme and the conductive support (Figure 10a).<sup>[216,218]</sup> For example, Kano and co-workers reported that a 2-methyl-1,4-naphthoquinone mediator and an  $\text{Fe}(\text{CN})_6^{4/3-}$  redox couple were used as electron transfer mediators

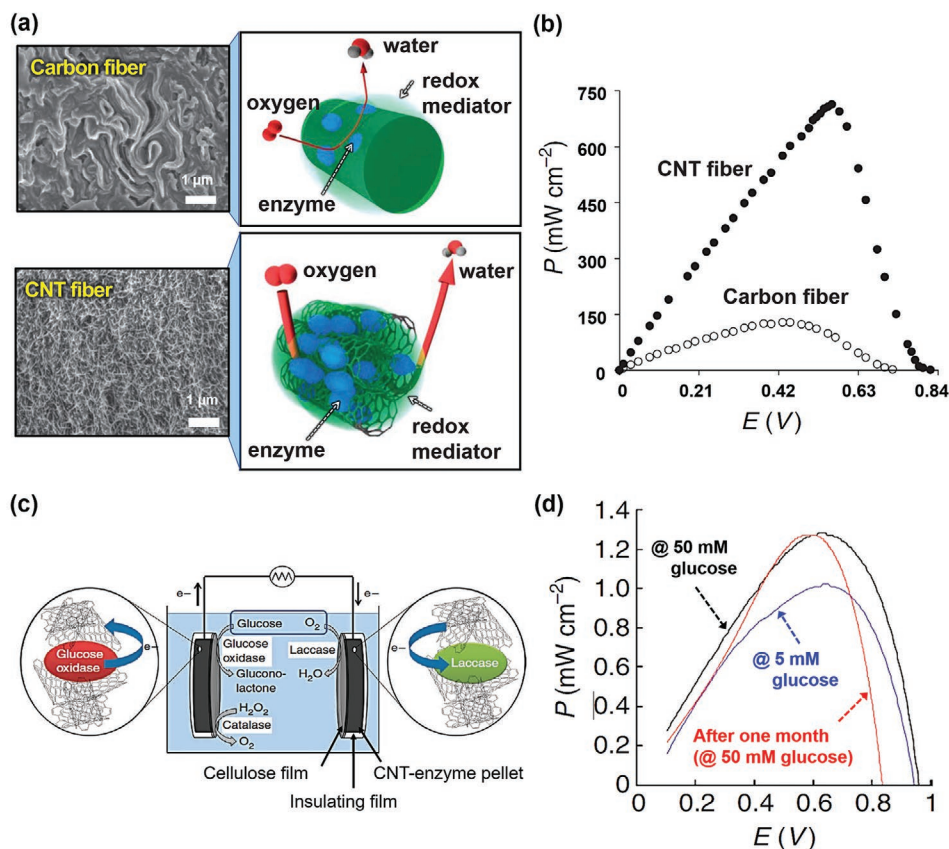


**Figure 9.** Carbon-material-based conventional BFCs. a) Classical carbon fiber BFC and porous CNT fiber BFC. b) Dependence of power density ( $P$ ) on operating voltage ( $V$ ) for two carbon material-based BFCs. a,b) Adapted with permission.<sup>[216]</sup> Copyright 2010, Springer Nature. c) CNT-enzyme disk-type BFCs. d) Power density performance of CNT-enzyme disk BFCs. c,d) Adapted with permission.<sup>[217]</sup> Copyright 2011, Springer Nature.



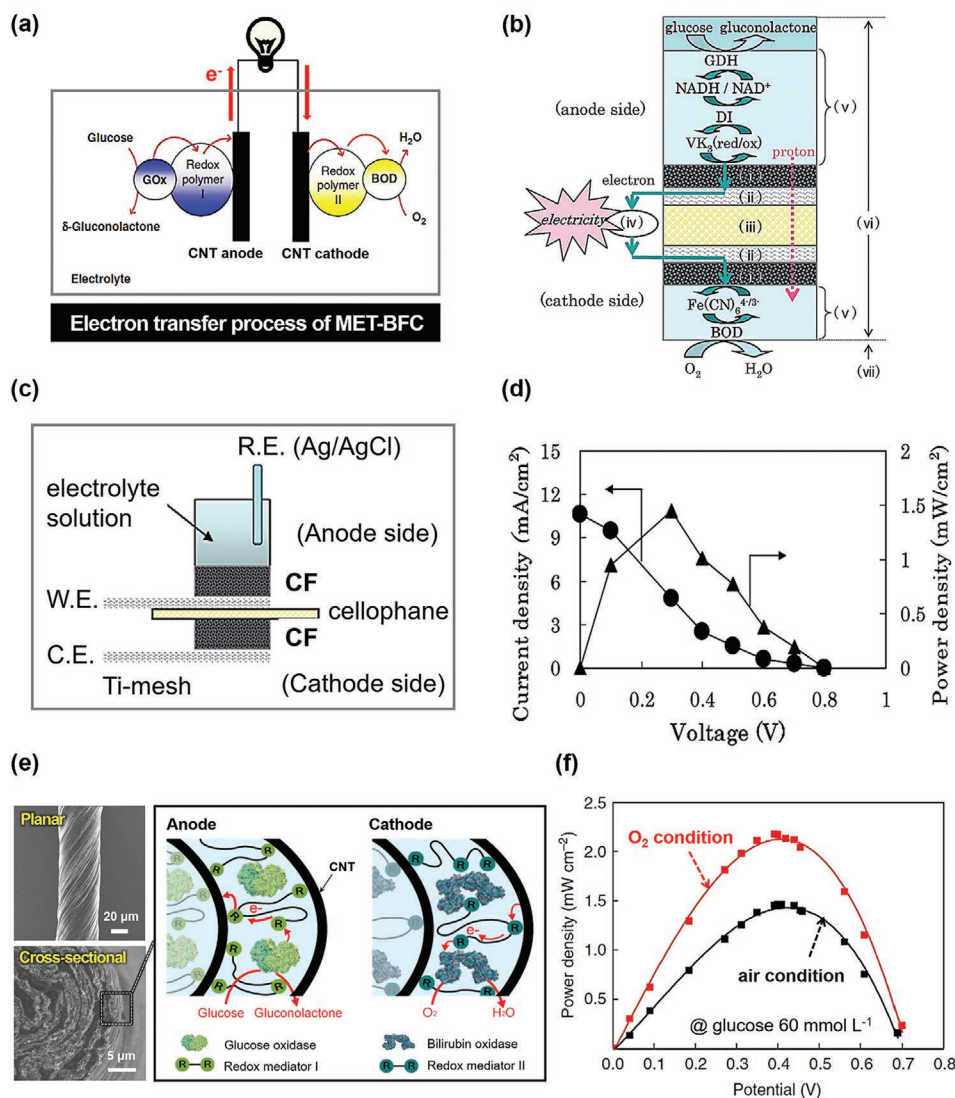


**Figure 10.** MET-BFCs. a) Schematic diagram of MET-BFCs. At the anode, electrons are transferred from glucose to glucose oxidase (GOx), from GOx to redox polymer (I) and from (I) to the CNT fiber. At the cathode, electrons are transferred from the CNT fiber to the redox polymer (II), from (II) to BOD and from BOD to oxygen. Adapted with permission.<sup>[216]</sup> Copyright 2010, Springer Nature. b) Schematic of the electron transfer reaction by shuttling electrons between electrodes and enzymes. (i) CNT fiber electrode, (ii) Ti-mesh collector, (iii) cellophane separator, (iv) external circuit, (v) enzyme/mediator immobilized layer, (vi) electrolyte solution including the phosphate buffer, and (vii) air. c) An electrochemical cell for a single BFC with a solution volume of 3 mL. d) The performance of a BFC composed of a CNT fiber-bioanode and a CNT fiber-biocathode. b–d) Adapted with permission.<sup>[219]</sup> Copyright 2009, The Royal Society of Chemistry. e) CNT yarn BFCs with osmium-based redox mediators, redox polymer I, for the anode and redox polymer II for the cathode. f) Power density for the complete BFC system at a 60 mmol L<sup>-1</sup> glucose concentration. e, f) Adapted with permission.<sup>[214]</sup> Copyright 2014, Springer Nature.

for the anode and cathode, respectively, which exhibited a maximum power output of  $\approx 1.45 \text{ mW cm}^{-2}$  (Figure 10b–d).<sup>[219]</sup> In particular, it was reported by many research groups that MET-BFCs using osmium complexes could significantly increase the electrocatalytic activity of enzymes.<sup>[220,221]</sup> Specifically, Kim and co-workers demonstrated that high-performance MET-BFCs could be realized by an osmium-based redox mediator that improves the electron transfer between enzymes and the host electrode (or conductive support).<sup>[214]</sup> In this case, two redox mediators of poly(*N*-vinylimidazole)-[Os(4,4'-dimethoxy-2,2'-bipyridine)<sub>2</sub>Cl]<sup>+2+</sup> and poly(acryl amide)-poly(*N*-vinylimidazole)-[Os(4,4'-dichloro-2,2'-bipyridine)<sub>2</sub>]<sup>+2+</sup>

were used for the anode and cathode, respectively (Figure 10e). This MET-BFC exhibited an extremely high power density of  $2.18 \text{ mW cm}^{-2}$  under oxygen-saturated, 60 mmol L<sup>-1</sup> glucose conditions (Figure 10f).<sup>[214]</sup>

However, despite this notable advantage, the presence of redox mediators including heavy metal ions in the MET-BFC electrode causes toxicity issues due to the leakage of redox mediators from the electrode, which may introduce toxicity issues after implantation. Therefore, considerable research interest has rapidly shifted from MET-BFCs to DET-BFCs in recent years, further focusing on enhancing the electron transfer efficiency of DET-BFCs.

#### 4.4. Incorporating Metal NPs into GOx for Electron Relay in DET-BFCs

A notable approach for efficient electron transfer in DET-BFCs is to incorporate metal NPs into GOx. Willner and co-workers demonstrated that metal NPs could act as an electron relay for both the enzyme alignment on the conductive support and the electrical wiring of the enzyme active center.<sup>[222–225]</sup> Therefore, GOx-based films containing Au NPs (i.e., Au–NP–GOx assemblies) could significantly enhance the electrochemical activity compared to native GOx films. Specifically, the incorporation of Au NPs into enzymes significantly enhanced the anodic current density

performance with increasing glucose concentration. Additionally, Willner and co-workers reported that a flavin-dependent GDH/Au NP-modified electrode (for DET-BFCs) exhibited improved electrocatalytic properties toward the oxidation of glucose because of the effective electrical contact between the GDH/Au NP and the electrode (Figure 11a–c).<sup>[225]</sup> In this case, the current density of the electrode gradually increased with increasing glucose concentration, and the electrode displayed a relatively high power output of  $\approx 32 \mu\text{W cm}^{-2}$  at a glucose concentration of  $200 \text{ mmol L}^{-1}$  even though it was a DET-BFC (Figure 11d,e). However, it is difficult to control the adsorption amount of Au NPs within the GOx film and to achieve homogeneous electron transfer efficiency of

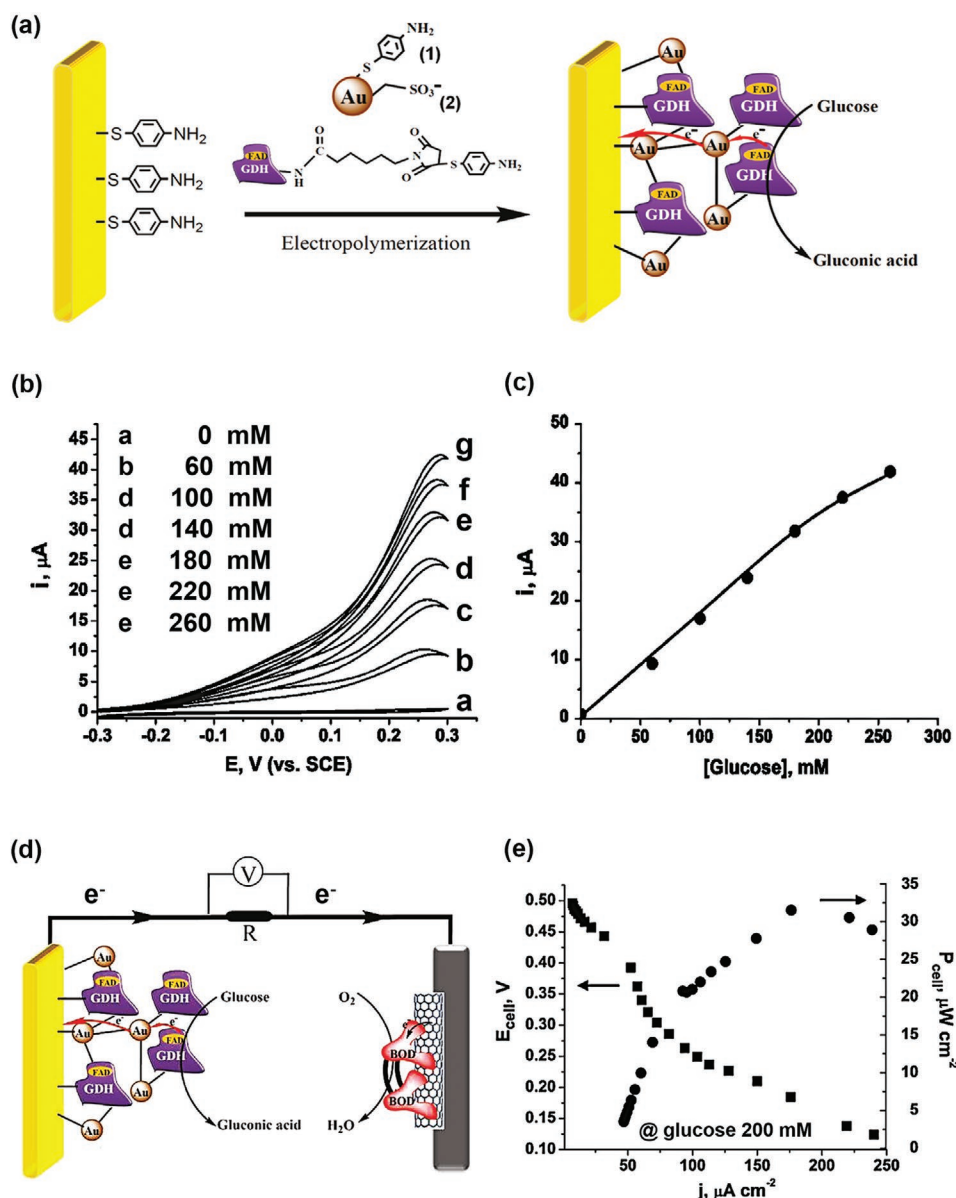


**Figure 11.** Au NP enzyme for DET-BFCs. a) GDH/Au NP composite-modified Au electrode. b) CVs corresponding to the oxidation of glucose. c) Calibration curve of the anodic current density levels at  $E = +0.3 \text{ V}$  versus SCE. d) Schematic presentation of the GDH/Au NP composite/BOD-CNT BFC. e) CVs corresponding to the oxidation of glucose by the GDH/Au NP composite-modified Au electrode. f) BFC power measured through different external resistance levels in air. a–f) Adapted with permission.<sup>[225]</sup> Copyright 2011, American Chemical Society.

the DET-BFC electrode with this approach. In this respect, the interfacial design and charge transfer kinetics between GOx and the metal NP should be further considered for improving the electrical communication of DET-BFC electrodes.<sup>[226]</sup>

#### 4.5. DET-BFC Cathodes Using Ligand Engineering

Cotton fibers composed of numerous cellulose microfibrils have attracted considerable attention in the area of electrodes for energy storage and conversion due to their large surface area and mechanically flexible properties. Recently, Cho and co-workers reported that cotton fibers can be completely converted to metallic cotton fibers (MCFs) using the LE-LbL assembly of TOA-Au NPs and a small-molecule linker (i.e., TREN) with an extremely low molecular weight ( $M_w \approx 146$ )<sup>[53]</sup> in organic media; furthermore, the formed MCFs can be effectively applied to both the host electrode and the BFC cathode with high ORR activity (Figure 12a).<sup>[227,228]</sup> To this end, the application of a dense and uniform coating of hydrophobic

TOA-Au NPs on highly porous cotton fibers was first realized by a consecutive ligand exchange reaction between pristine bulky ligands (i.e., TOA ligands) loosely bound to the surface of Au NPs and TREN. With an increasing bilayer number ( $n$ ) of LE-LbL-assembled (TOA-Au NP/TREN) $_n$  multilayers onto cotton fibers up to  $n = 20$ , the electrical conductivity was measured to be  $\approx 3.5 \times 10^3 \text{ S cm}^{-1}$ , and a low resistivity of  $\approx 1.2 \times 10^{-4} \Omega \text{ cm}$  was measured (in this case, the outermost layer of the resultant MCFs was TREN) (Figure 12b).

On the other hand, the porous structure, mechanical flexibility, and intrinsic characteristics of cotton fibers were well preserved even after the successive mass loading of Au NP layers (i.e., Au NP/TREN). Furthermore, it should be noted that MCFs with highly porous structures can allow facile ion (electrolyte) transport. In addition to the role of MCFs as a host electrode, the (TOA-Au NP/TREN) $_{20}$ -coated cotton fibers exhibited notable ORR activity originating from the Au NPs, inducing a high cathodic current density of  $-10.0 \text{ mA cm}^{-2}$  in pH 7.4 phosphate buffer solution (PBS) under ambient conditions (Figure 12c). Interestingly, this ORR activity could be

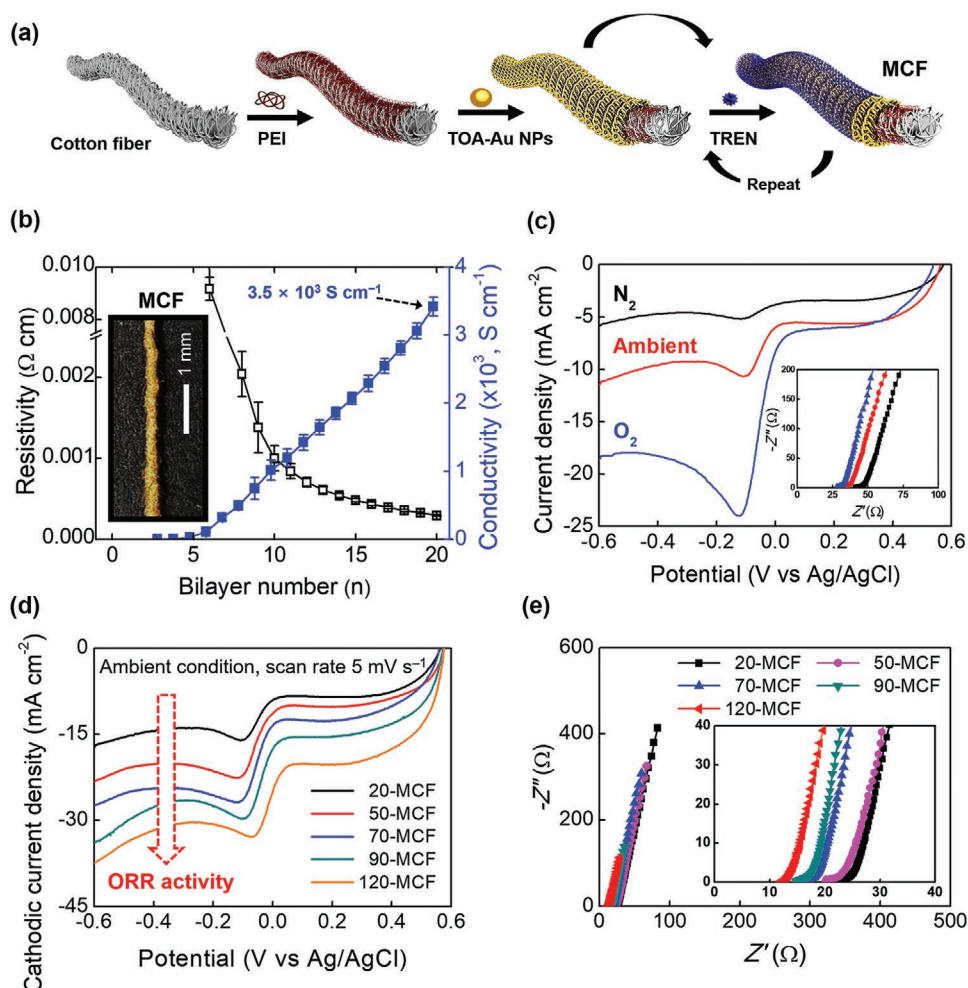


**Figure 12.** Ligand-engineering-based cathodes. a) Illustration of MCF electrode-based BFCs. b) Resistivity and electrical conductivity of  $n$ -MCFs as a function of  $n$ . Inset: Optical image of metallic cotton fibers (20-MCFs). c) Cathodic performance curves. Inset: Nyquist plots of a 20-MCF in PBS under  $\text{N}_2$ , ambient, and  $\text{O}_2$  conditions. d) Cathodic current density performance for  $n$ -MCF cathodes as a function of  $n$ . e) Nyquist plots of the MCF cathodes depending on  $n$ . a–e) Adapted under the terms of the CC-BY Creative Commons Attribution 4.0 International license (<https://creativecommons.org/licenses/by/4.0/>).<sup>[53]</sup> Copyright 2018, The Authors, published by Springer Nature.

**Table 1.** Power output performance of various BFCs reported to date.

Host electrode	Catalysts <sup>b)</sup> Anode/cathode	Fuel Anode/cathode	$P_{\max}$ [mW cm <sup>-2</sup> ]	Refs.
MCF <sup>a)</sup>	GOx/Au NP	Glucose/O <sub>2</sub>	3.7 (ambient cond.)	[53]
CNT fiber	GOx/BOD	Glucose/O <sub>2</sub>	0.74 (air cond.)	[216]
CNT yarn	GOx/BOD	Glucose/O <sub>2</sub>	2.18 (oxygen cond.)	[214]
CNT film	GOx/Pt <sub>bulk</sub> <sup>c)</sup>	Glucose/O <sub>2</sub>	1.34 (air cond.)	[233]
Compressed CNTs	GOx-Cat/Lac	Glucose/O <sub>2</sub>	1.25	[217]
3D Au NP (on carbon paper)	FDH/BOD	Fructose/O <sub>2</sub>	0.87 (oxygen cond.)	[237]
SWNT (on glassy carbon)	GDH/Lac	Glucose/O <sub>2</sub>	0.0095 (ambient cond.)	[238]
Graphene/Au NP Hybrid (on Au substrate)	FDH/Lac	Formic acid/O <sub>2</sub>	1.96	[239]
Nafion/poly(vinyl pyrrolidone) compound nanowire (on Au electrode)	GOx/Lac	Glucose/O <sub>2</sub>	0.03	[240]
Catecholamine polymers (on Au disk)	GOx/carbon rod	Glucose/O <sub>2</sub>	1.62 (KMnO <sub>4</sub> + H <sub>2</sub> SO <sub>4</sub> )	[241]
Au NP/PANI (polyaniline) network (on glassy carbon)	GOx/Lac	Glucose/O <sub>2</sub>	0.685	[242]
Enzyme cluster composite (on carbon paper)	GOx/Pt <sub>bulk</sub> <sup>c)</sup>	Glucose/O <sub>2</sub>	1.62	[243]

<sup>a)</sup>MCF, metallic cotton fiber; <sup>b)</sup>The abbreviations for different enzymes: glucose oxidase (GOx), laccase (Lac), bilirubin oxidase (BOD), fructose dehydrogenase (FDH), and catalase (Cat); <sup>c)</sup>Pt<sub>bulk</sub>: Commercial Pt bulk electrode.

further intensified according to the deposition bilayer number (up to  $n = 120$ ) of the Au NP layers (Figure 12d,e). These results demonstrate that the LE-LbL assembly of electrocatalytic NPs is highly efficient in developing high-performance cathode electrodes as well as host electrodes in DET-BFCs.

#### 4.6. DET-BFC Anode Using Ligand Engineering and Small-Molecule Linkers

Most conventional BFC anodes (i.e., MET- and DET-BFC anodes) have been prepared through simple physical adsorption of GOx enzymes onto carbon supports (or host electrodes). Therefore, the reported approaches have much difficulty than the proposed approach in precisely controlling the interfacial distance, interactions, conformation, and stability between enzymes and host electrodes as well as the enzyme loading amount, which strongly restricts the effective utilization of electrochemical enzyme reactions.<sup>[229–233]</sup>

Recently, it was reported that a GOx-coated MCF (i.e., Au NP-coated cotton fiber) for a DET-BFC anode could be successfully prepared by electrostatic LbL assembly of anionic GOx and cationic TREN.<sup>[53]</sup> In this case, the highly porous MCFs with an outermost TREN layer (see Section 4.5.) could be electrostatically bonded with anionic GOx at pH 7.4 because the NH<sub>2</sub> groups of the outermost TREN layer were converted to positively charged amine groups in pH 7.4 PBS. As a result, ligand-engineering- and LbL-assembly-based BFC anodes had high current output (31.6 mA cm<sup>-2</sup>) in 300 mmol L<sup>-1</sup> glucose-containing PBS at +0.6 V (Figure 13a). Particularly, when the apparent heterogeneous electron transfer rate ( $K_s$ ) was estimated by the Laviron method for a surface-controlled electrochemical system, the (GOx/TREN)<sub>30</sub>-coated MCF anode exhibited a larger  $K_s$  value of  $6.0 \pm 0.1$  s<sup>-1</sup> than that of the CNT-modified anode or TMO NP-based anode (1.53 s<sup>-1</sup> for the multiwalled nanotube (MWNT)-modified electrode, 3.96 s<sup>-1</sup> for the porous TiO<sub>2</sub> electrode).<sup>[234–236]</sup> It should be noted that the TREN-based MCF electrode with a large  $K_s$  is significantly

effective in facilitating the direct electron transfer of GOx. The authors also suggested that this high anodic performance was mainly caused by the high electrical conductivity of the host electrode and the minimized distance between neighboring GOx layers with the aid of small-molecule linkers (i.e., TREN).

To demonstrate these possibilities, the authors prepared (GOx/PEI)<sub>*n*</sub> multilayer-coated MCFs using the bulky insulating compound poly(ethylene imine) (PEI,  $M_w \approx 25\,000$ ) instead of TREN, which was LbL-assembled with GOx on MCFs, and then they investigated the anodic performance (Figure 13a,b). In this case, the electrochemical performance of the (GOx/TREN)<sub>*n*</sub>-coated MCF anodes (i.e., a low anodic areal current density, a high internal resistance and a low ion-diffusion rate). Furthermore, full-cell DET-BFCs composed of an enzyme-free MCF cathode and a (GOx/TREN)<sub>*n*</sub>-coated MCF anode exhibited a considerably high power density of 3.7 mW cm<sup>-2</sup>, outperforming conventional BFCs, including DET- and MET-BFCs (Figure 13c–e and Table 1).

As a result, this ligand-engineering-based interfacial design for the preparation of BFC electrodes (i.e., cathodes and anodes) could convert various substrates such as textiles and cotton fibers into highly conductive host electrodes and significantly improve the electron communication between the electrode and enzymes due to the notable decrease in the electron transfer resistance at all heterogeneous interfaces. In this regard, a ligand engineering approach can provide a basic platform for developing high-performance BFC electrodes with high power output and excellent operational stability.

## 5. Conclusion and Outlook

Ligand engineering is one of the classical topics in determining the size, shape, and dispersion stability of functional NPs in desired solutions. In most cases, high-quality inorganic NPs (in terms of crystallinity, size, and shape) have been synthesized using a variety of bulky hydrophobic ligands such as TOA or

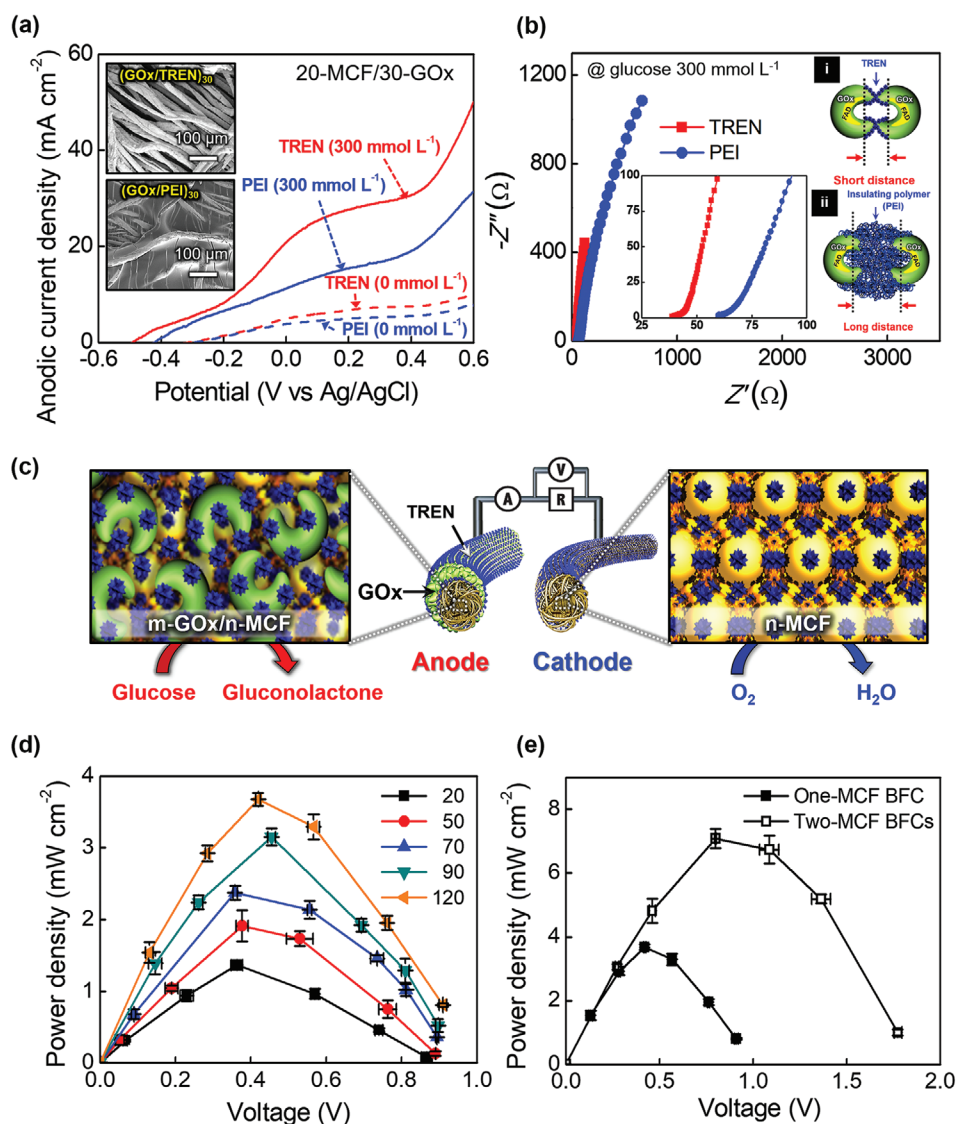


**Figure 13.** Ligand-engineering-based anodes and complete BFCs. a) Anodic current density performance of 30-GOx/20-MCF electrodes prepared from (GOx/TREN)<sub>30</sub> and (GOx/PEI)<sub>30</sub> multilayered MCFs. Inset: FE-SEM images of (GOx/TREN)<sub>30</sub> and (GOx/PEI)<sub>30</sub> multilayered MCF anodes. b) Nyquist plots of TREN- and PEI-based 30-GOx/20-MCF anodes. Inset: Schematic diagram showing the difference between the small-molecule linker (TREN) (i) and the insulating polymer linker (PEI) (ii), which is related to the internal distance. c) Redox process for a complete MCF-BFC composed of a cathode and an anode through an external load resistor. d) Power outputs of MCF-BFCs (an n-MCF cathode and a 30-bilayer GOx/TREN multilayer-coated MCF anode) with external resistors (1 kΩ ≈ 10 MΩ) as a function of n-MCF. e) Power outputs of one and two MCF-BFCs composed of the 120-MCF cathode and the 30-GOx/20-MCF anode. In these cases, the two MCF-BFCs were connected with each other in series. a–e) Adapted under the terms of the CC-BY Creative Commons Attribution 4.0 International license (<https://creativecommons.org/licenses/by/4.0/>).<sup>[53]</sup> The Authors, published by Springer Nature.

organic fatty acid ligands (OA, PA, and linoleic acid ligands) in nonpolar media. However, it is difficult for these hydrophobic NPs to stably and uniformly adsorb onto hydrophilic substrates with the desired size and shape. Furthermore, when fabricating bulk electrodes from hydrophobic NPs such as metal or TMO NPs, the bulky native ligands bound to the surface of NPs seriously restrict the charge transfer between neighboring NPs as well as between current collectors and NPs, resulting in poor utilization of functional NPs with intrinsically outstanding electrical and/or electrochemical properties. Thus, these organic ligands play a critical role in determining the performance of NP-based electrodes in various electrochemical energy storage and conversion devices.

From this viewpoint, we have discussed the need for a unique ligand engineering approach using LE-LbL assembly in organic media. In particular, amine-functionalized organic linkers used in the LE-LbL assembly method could almost completely remove the bulky native ligands bound to the surface of metal and TMO NPs and could bridge all interfaces of electrodes (i.e., substrate/metal NP, metal NP/metal NP, and metal NP/TMO NP) for energy storage. Furthermore, we have highlighted that the LE-LbL assembly method allows the application of a highly uniform coating of functional NPs over the entire area of porous substrates, such as paper and thread-type cotton, without any NP agglomeration or pore blocking. It should be noted that this approach is completely different



**Figure 14.** Potential applications of the NP-based energy electrodes prepared by ligand-exchange-induced LbL assembly in the field of wearable, portable, and biomedical electronics.

from conventional LbL assemblies based on complementary interactions (i.e., electrostatic attraction, hydrogen bonding, or covalent bonding) between organic ligands and bulky polymer linkers without any ligand exchange reaction.

As a result, the LE-LbL assembly using small organic linkers could significantly enhance the charge transfer kinetics between neighboring NPs as well as between the substrate and functional NPs while maintaining the mechanical flexibility of porous substrates. These phenomena were confirmed by the notable performance improvement in the various LE-LbL-assembled electrodes for batteries, electrochemical capacitors and BFCs. Considering that this approach can be effectively applied to various conductive and electrochemically active materials irrespective of substrate size and shape, we suggest that our approach can provide an important basis for developing high-performance electrodes for energy storage that require a large active surface area, a flexibility similar to textiles, and precise control over the thickness or loading mass. Finally, the ligand control approach can potentially transform the assembly method of NPs into a highly controllable process that can produce structure- and property-tuned 3D bulk electrodes for various electrochemical energy storage and conversion systems.

Despite such powerful advantages of the LE-LbL assembly, which allows accurate control of the interfacial interaction and the loading amount (or film thickness) of the active NPs within the electrode, thin film (nanometer-thick) deposition by dip coating process often creates time-consuming issues in preparing energy storage system with high areal performance (i.e., mass loading of NP). Basically, these issues, including process time and NP loading, can easily be optimized with simple control of solution

concentration.<sup>[50,244]</sup> More potentially, the ligand engineering approach can be expanded to large-scale LbL assemblies such as automatic spray deposition and roll-to-roll processes, which can significantly reduce the electrode fabrication time (few seconds per layer) while achieving the mass loading of total amount of energy material on various highly porous substrates, enabling the production of industrial-grade energy electrodes.<sup>[134,245]</sup> In this regard, an effective combination between the ligand-exchange-induced interface design of functional nanomaterials and the advanced fabrication technology can be a breakthrough in overcoming barriers to applying the LbL assembly to practical devices. Therefore, we envision that such an approach can be widely and effectively applied to the energy electrodes for various wearable/portable devices, including energy storage, conversion devices and biomedical devices (Figure 14).

### Acknowledgements

This work was supported by a National Research Foundation (NRF) grant funded by the Ministry of Science, ICT & Future Planning (MSIP) (2019R1A4A1027627; 2018R1A2A1A05019452; 2016M3A7B4910619) and the Basic Science Research Program through the National Research Foundation of Korea (NRF) funded by the Ministry of Education (NRF-2017R1A6A3A04003192). This work was also supported by the DGIST R&D Programs of the Ministry of Science and ICT of Korea (20-ET-08).

### Conflict of Interest

The authors declare no conflict of interest.

## Author Contributions

Y.K. and C.H.K. contributed equally to this work. Y.K., C.H.K., S.W.L., and J.C. wrote and revised the manuscript. All authors discussed the results and commented on the manuscript.

## Keywords

energy electrodes, energy nanoparticles, layer-by-layer assembly, multilayers

Received: March 20, 2020

Revised: May 2, 2020

Published online: September 21, 2020

- [1] J. M. Tarascon, M. Armand, *Nature* **2001**, 414, 359.
- [2] P. Simon, Y. Gogotsi, *Nat. Mater.* **2008**, 7, 845.
- [3] B. Duun, H. Kamath, J.-M. Tarascon, *Science* **2011**, 334, 928.
- [4] V. Etacheri, R. Marom, R. Elazari, G. Salitra, D. Aurbach, *Energy Environ. Sci.* **2011**, 4, 3243.
- [5] C. Liu, F. Li, L. P. Ma, H. M. Cheng, *Adv. Mater.* **2010**, 22, E28.
- [6] A. S. Arico, P. Bruce, B. Scrosati, J. M. Tarascon, W. Van Schalkwijk, *Nat. Mater.* **2005**, 4, 366.
- [7] B. C. H. Steele, A. Heinzl, *Nature* **2001**, 414, 345.
- [8] S. C. Barton, J. Gallaway, P. Atanassov, *Chem. Rev.* **2004**, 104, 4867.
- [9] X. Yu, S. Yun, N. S. Yeon, P. Bhattacharya, L. Wang, S. W. Lee, X. Hu, H. S. Park, *Adv. Energy Mater.* **2018**, 8, 1702930.
- [10] E. Frachowiak, F. Béguin, *Carbon* **2001**, 39, 937.
- [11] H. Ji, X. Zhao, Z. Qiao, J. Jung, Y. Zhu, Y. Lu, L. L. Zhang, A. H. MacDonald, R. S. Ruoff, *Nat. Commun.* **2014**, 5, 3317.
- [12] S. W. Lee, B. M. Gallant, H. R. Byon, P. T. Hammond, Y. Shao-Horn, *Energy Environ. Sci.* **2011**, 4, 1972.
- [13] S. W. Lee, N. Yabuuchi, B. M. Gallant, S. Chen, B.-S. Kim, P. T. Hammond, Y. Shao-Horn, *Nat. Nanotechnol.* **2010**, 5, 531.
- [14] Y. Wang, Y. Song, Y. Xia, *Chem. Soc. Rev.* **2016**, 45, 5925.
- [15] P. L. Taberna, S. Mitra, P. Poizot, J.-M. Tarascon, *Nat. Mater.* **2006**, 5, 567.
- [16] H. Chen, L. F. Hu, M. Chen, Y. Yan, L. M. Wu, *Adv. Funct. Mater.* **2014**, 24, 934.
- [17] S.-H. Yu, S. H. Lee, D. J. Lee, Y.-E. Sung, T. Hyeon, *Small* **2016**, 12, 2146.
- [18] S. Chen, J. Zhu, X. Wu, Q. Han, X. Wang, *ACS Nano* **2010**, 4, 2822.
- [19] B. Ammundsen, J. Paulsen, *Adv. Mater.* **2001**, 13, 943.
- [20] X. C. Dong, H. Zu, X. W. Wang, Y. X. Huang, M. B. Chan-Park, H. Zhang, L. H. Wang, W. Huang, P. Chen, *ACS Nano* **2012**, 6, 3206.
- [21] Z. S. Wu, W. C. Ren, L. Wen, L. B. Gao, J. P. Zhao, Z. P. Chen, G. M. Zhou, F. Li, H. M. Cheng, *ACS Nano* **2010**, 4, 3187.
- [22] C. He, S. Wu, N. Zhao, C. Shi, E. Liu, J. Li, *ACS Nano* **2013**, 7, 4459.
- [23] W.-M. Zhang, X.-L. Wu, J.-S. Hu, Y.-G. Guo, L.-J. Wan, *Adv. Funct. Mater.* **2008**, 18, 3941.
- [24] B. E. Conway, *Electrochemical Supercapacitor: Scientific Fundamentals and Technological Applications*, Plenum Publishers, New York **1999**.
- [25] V. Augustyn, P. Simon, B. Dunn, *Energy Environ. Sci.* **2014**, 7, 1597.
- [26] P. Poizot, S. Laruelle, S. Grugéon, L. Dupont, J.-M. Tarascon, *Nature* **2000**, 407, 496.
- [27] I. E. Rauda, V. Augustyn, B. Dunn, S. H. Tolbert, *Acc. Chem. Res.* **2013**, 46, 1113.
- [28] P. Ragupathy, D. H. Park, G. Campet, N. H. Vasan, S.-J. Hwang, J.-H. Choy, N. Munichandraiah, *J. Phys. Chem. C* **2009**, 113, 6303.
- [29] R. Malik, D. Burch, M. Bazant, G. Ceder, *Nano Lett.* **2010**, 10, 4123.
- [30] H.-W. Lee, P. Muralidharan, R. Ruffo, C. M. Mari, Y. Cui, D. K. Kim, *Nano Lett.* **2010**, 10, 3852.
- [31] A. E. Fischer, M. P. Saunders, K. A. Pettigrew, D. R. Rolison, J. W. Long, *J. Electrochem. Soc.* **2008**, 155, A246.
- [32] S. Wu, B. Yu, Z. Wu, S. Fang, B. Shi, J. Yang, *RSC Adv.* **2018**, 8, 8544.
- [33] G. He, L. F. Nazar, *Nano Lett.* **2017**, 2, 1122.
- [34] J. W. Kim, V. Augustyn, B. Dunn, *Adv. Energy Mater.* **2012**, 2, 141.
- [35] Z.-S. Wu, G. Zhou, L.-C. Yin, W. Ren, F. Li, H.-M. Cheng, *Nano Energy* **2012**, 1, 107.
- [36] H. Tabassum, R. Zou, A. Mahmood, Z. Liang, Q. Wang, H. Zhang, S. Gao, C. Qu, W. Guo, S. Guo, *Adv. Mater.* **2018**, 30, 1705441.
- [37] J. C. Park, J. Kim, H. Kwon, H. Song, *Adv. Mater.* **2009**, 21, 803.
- [38] M. A. Boles, D. Ling, T. Hyeon, D. V. Talapin, *Nat. Mater.* **2016**, 15, 141.
- [39] B. D. Clark, C. J. DeSantis, G. Wu, D. Renard, M. J. McClain, L. Bursi, A.-L. Tsai, P. Nordlander, N. J. Halas, *J. Am. Chem. Soc.* **2019**, 141, 1716.
- [40] K. J. Si, Q. Shi, W. Cheng, *Adv. Sci.* **2018**, 5, 1700179.
- [41] S. Lee, Y. Song, Y. Ko, Y. Ko, J. Ko, C. H. Kwon, J. Huh, S.-W. Kim, B. Yeom, J. Cho, *Adv. Mater.* **2020**, 32, 1906460.
- [42] S. Kang, D. Nam, J. Choi, J. Ko, D. Kim, C. H. Kwon, J. Huh, J. Cho, *ACS Appl. Mater. Interfaces* **2019**, 11, 12032.
- [43] I. Cho, H. Jung, B. G. Jeong, J. H. Chang, Y. Kim, K. Char, D. C. Lee, C. Lee, J. Cho, W. K. Bae, *ACS Nano* **2017**, 11, 684.
- [44] Z.-Y. Zhou, X. Kang, Y. Song, S. Chen, *J. Phys. Chem. C* **2012**, 116, 10592.
- [45] L. M. Rossi, J. L. Fiorio, M. A. S. Garcia, C. P. Ferraz, *Dalton Trans.* **2018**, 47, 5889.
- [46] D. Ling, M. J. Hackett, T. Hyeon, *Nano Today* **2014**, 9, 457.
- [47] G. H. Woehrle, J. E. Hutchison, *Inorg. Chem.* **2005**, 44, 6149.
- [48] J. S. Owen, J. Park, P.-E. Trudeau, A. P. Alivisatos, *J. Am. Chem. Soc.* **2008**, 130, 12279.
- [49] A. Dong, X. Ye, J. Chen, Y. Kang, T. Gordon, J. M. Kikkawa, C. B. Murray, *J. Am. Chem. Soc.* **2011**, 133, 998.
- [50] Y. Ko, H. Baek, Y. Kim, M. Yoon, J. Cho, *ACS Nano* **2013**, 7, 143.
- [51] M. Yoon, J. Choi, J. Cho, *Chem. Mater.* **2013**, 25, 1735.
- [52] Y. Ko, M. Kwon, W. K. Bae, B. Lee, S. W. Lee, J. Cho, *Nat. Commun.* **2017**, 8, 536.
- [53] C. H. Kwon, Y. Ko, D. Shin, M. Kwon, J. Park, W. K. Bae, S. W. Lee, J. Cho, *Nat. Commun.* **2018**, 9, 4479.
- [54] Y. Ko, D. Shin, B. Koo, S. W. Lee, W.-S. Yoon, J. Cho, *Nano Energy* **2015**, 12, 612.
- [55] Y. Song, D. Kim, S. Kang, Y. Ko, J. Ko, J. Huh, Y. Ko, S. W. Lee, J. Cho, *Adv. Funct. Mater.* **2019**, 29, 1806584.
- [56] C. H. Kwon, Y. Ko, D. Shin, S. W. Lee, J. Cho, *J. Mater. Chem. A* **2019**, 7, 13495.
- [57] Y. Ko, D. Kim, C. H. Kwon, J. Cho, *Appl. Surf. Sci.* **2018**, 436, 791.
- [58] D. Shin, Y. Ko, J. Cho, *RSC Adv.* **2016**, 6, 21844.
- [59] M. Park, Y. Kim, Y. Ko, S. Cheong, S. W. Ryu, J. Cho, *J. Am. Chem. Soc.* **2014**, 136, 17213.
- [60] D. Kim, S. Cheong, Y. G. Ahn, S. W. Ryu, J.-K. Kim, J. Cho, *Nanoscale* **2016**, 8, 7000.
- [61] S. Sivaramakrishnan, P.-J. Chia, Y.-C. Yeo, L.-L. Chua, P. K.-H. Ho, *Nat. Mater.* **2007**, 6, 149.
- [62] J. A. Rodriguez, J. Hrbek, *Acc. Chem. Res.* **1999**, 32, 719.
- [63] G. E. Poirier, E. D. Pylant, *Science* **1996**, 272, 1145.
- [64] F. Dubois, B. Mahler, B. Dubertret, E. Doris, C. Mioskowski, *J. Am. Chem. Soc.* **2007**, 129, 482.
- [65] B. T. Anto, S. Sicaramakrishnan, L.-L. Chua, P. K.-H. Ho, *Adv. Funct. Mater.* **2010**, 20, 296.
- [66] B. M. Amoli, S. Gumfekar, A. Hu, Y. N. Zhou, B. Zhao, *J. Mater. Chem.* **2012**, 22, 20048.
- [67] M. Brust, D. Bethell, C. J. Kiely, D. J. Schiffrin, *Langmuir* **1998**, 14, 5425.

- [68] A. T. Fafarman, S.-H. Hong, S. J. Oh, H. Caglayan, X. Ye, B. T. Diroll, N. Engheta, C. B. Murray, C. R. Kagan, *ACS Nano* **2014**, *8*, 2746.
- [69] P. Pulkkinen, J. Shan, K. Leppänen, A. Känsäkoski, A. Laiho, M. Järn, H. Tenhu, *ACS Appl. Mater. Interfaces* **2009**, *1*, 519.
- [70] L. V. Govor, G. H. Bauer, G. Reiter, J. Parisi, *Phys. Rev. B* **2010**, *82*, 155437.
- [71] F.-C. Chiu, *Adv. Mater. Sci. Eng.* **2014**, *7*, 1.
- [72] U. Simon, *Adv. Mater.* **1998**, *10*, 1487.
- [73] R. H. Terrill, T. A. Postlethwaite, C.-h. Chen, C.-D. Poon, A. Terzis, A. Chen, J. E. Hutchison, M. R. Clark, G. Wignall, J. D. Londono, R. Superfine, M. Falvo, C. S. Johnson, Jr., E. T. Samulski, R. W. Murray, *J. Am. Chem. Soc.* **1995**, *117*, 12537.
- [74] W. P. Weulfing, S. J. Green, J. J. Pietron, D. E. Cliffler, R. W. Murray, *J. Am. Chem. Soc.* **2000**, *122*, 11465.
- [75] G. Markovich, C. P. Collier, J. M. Heath, *Phys. Rev. Lett.* **1998**, *80*, 3807.
- [76] G. Schön, U. Simon, *Colloid Polym. Sci.* **1995**, *273*, 101.
- [77] D. Deng, Y. Jin, Y. Cheng, T. Qi, F. Xiao, *ACS Appl. Mater. Interfaces* **2013**, *5*, 3839.
- [78] Y. J. Lee, C. Lee, H. M. Lee, *Nanotechnology* **2018**, *29*, 055602.
- [79] L. Zhong, C. Beaudette, J. Guo, K. Bozhilov, L. Mangolini, *Sci. Rep.* **2016**, *6*, 30952.
- [80] J. Ederth, P. Heszler, A. Hultåker, G. A. Niklasson, C. G. Granqvist, *Thin Solid Films* **2003**, *445*, 199.
- [81] Y. H. Jo, I. Jung, C. S. Choi, I. Kim, H. M. Lee, *Nanotechnology* **2011**, *22*, 225701.
- [82] S. Pradhan, D. Ghosh, L.-P. Xu, S. Chen, *J. Am. Chem. Soc.* **2007**, *129*, 10622.
- [83] A. Ghosh, S. Basak, B. H. Wunsch, R. Kumar, F. Stellacci, *Angew. Chem., Int. Ed.* **2011**, *50*, 7900.
- [84] L. Lu, S. Zou, Y. Zhou, J. Liu, R. Li, Z. Xu, L. Xiao, J. Fan, *Catal. Sci. Technol.* **2018**, *8*, 746.
- [85] L. Lu, B. Lou, S. Zou, H. Kobayashi, J. Liu, L. Xiao, J. Fan, *ACS Catal.* **2018**, *8*, 8484.
- [86] J. A. Smith, P. K. Jain, *J. Am. Chem. Soc.* **2016**, *138*, 6765.
- [87] I. Cho, Y. Song, S. Cheong, Y. Kim, J. Cho, *Small* **2020**, *16*, 1906768.
- [88] J. Yun, Y. Song, I. Cho, Y. Ko, C. H. Kwon, J. Cho, *Nanoscale* **2019**, *11*, 17815.
- [89] H. Yang, W. Fan, A. Vaneski, A. S. Susha, W. Y. Teoh, A. L. Rogach, *Adv. Funct. Mater.* **2012**, *22*, 2821.
- [90] T. Rajh, L. X. Chen, K. Lukas, T. Liu, M. C. Thurnauer, D. M. Tiede, *J. Phys. Chem. B* **2002**, *106*, 10543.
- [91] J. Choi, D. Nam, D. Shin, Y. Song, C. H. Kwon, I. Cho, S. W. Lee, J. Cho, *ACS Nano* **2019**, *13*, 12719.
- [92] B. Y. Ahn, E. B. Duoss, M. J. Motala, X. Guo, S.-I. Park, Y. Xiong, J. Yoon, R. G. Nuzzo, J. A. Rogers, J. A. Lewis, *Science* **2009**, *323*, 1590.
- [93] S. Magdassi, M. Grouchko, O. Berezin, A. Kamysny, *ACS Nano* **2010**, *4*, 1943.
- [94] Y. Kim, J. Zhu, B. Yeom, M. D. Prima, X. Su, J.-G. Kim, S. J. Yoo, C. Uher, N. A. Kotov, *Nature* **2013**, *500*, 59.
- [95] G. Decher, *Science* **1997**, *277*, 1232.
- [96] F. Caruso, R. A. Caruso, H. Möhwald, *Science* **1998**, *282*, 1111.
- [97] J. Cho, K. Char, J.-D. Hong, K.-B. Lee, *Adv. Mater.* **2001**, *13*, 1076.
- [98] J.-S. Lee, J. Cho, C. Lee, I. Kim, J. Park, Y. Kim, H. Shin, J. Lee, F. Caruso, *Nat. Nanotechnol.* **2007**, *2*, 790.
- [99] Y. Kim, C. Lee, I. Shim, D. Wang, J. Cho, *Adv. Mater.* **2010**, *22*, 5140.
- [100] S. Lee, B. Lee, B. J. Kim, J. Park, W. K. Bae, K. Char, C. J. Hawker, J. Bang, J. Cho, *J. Am. Chem. Soc.* **2009**, *131*, 2579.
- [101] Y. Ko, Y. Kim, H. Baek, J. Cho, *ACS Nano* **2011**, *5*, 9918.
- [102] K. Ariga, E. Ahn, M. Park, B.-S. Kim, *Chem. - Asian J.* **2019**, *14*, 2553.
- [103] Q. An, T. Huang, F. Shi, *Chem. Soc. Rev.* **2018**, *47*, 5061.
- [104] Y. Ko, M. Kwon, Y. Song, S. W. Lee, J. Cho, *Adv. Funct. Mater.* **2018**, *28*, 1804926.
- [105] L. Fabbrizzi, A. Poggi, *Chem. Soc. Rev.* **2013**, *42*, 1681.
- [106] N. C. Anderson, M. P. Hendricks, J. J. Choi, J. S. Owen, *J. Am. Chem. Soc.* **2013**, *135*, 18536.
- [107] S. Sun, *Adv. Mater.* **2006**, *18*, 393.
- [108] Y. Wang, K. Sentosum, A. Li, M. Coronado-Puchau, A. Sánchez-Iglesias, S. Li, X. Su, S. Bals, L. M. Liz-Marzán, *Chem. Mater.* **2015**, *27*, 8032.
- [109] M. J. Hostetler, A. C. Templeton, R. W. Murray, *Langmuir* **1999**, *15*, 3782.
- [110] R. R. Kolega, J. B. Schlenoff, *Langmuir* **1998**, *14*, 5469.
- [111] K. Nomiyama, S. Yamamoto, R. Noguchi, H. Yokoyama, N. C. Kasuga, K. Ohyama, C. Kato, *J. Inorg. Biochem.* **2003**, *95*, 208.
- [112] Y. Zhou, S. L. Candelaria, Q. Liu, Y. Huang, E. Uchaker, G. CaO, *J. Mater. Chem. A* **2014**, *2*, 8472.
- [113] T. Liu, K. Wang, Y. Chen, S. Zhao, Y. Han, *Green Energy Environ.* **2019**, *4*, 171.
- [114] X. Zhang, W. Shi, J. Zhu, D. J. Kharistal, W. Zhao, B. S. Lalia, H. H. Hng, Q. Yan, *ACS Nano* **2011**, *5*, 2013.
- [115] D. Lin, Z. Lu, P.-C. Hsu, H. R. Lee, N. Liu, J. Zhao, H. Wang, C. Liu, Y. Cui, *Energy Environ. Sci.* **2015**, *8*, 2371.
- [116] K. Saravanan, K. Ananthanarayanan, P. Balaya, *Energy Environ. Sci.* **2010**, *3*, 939.
- [117] H. Zhao, Y. Wei, R. Qiao, C. Zhu, Z. Zheng, M. Ling, Z. Jie, Y. Bai, Y. Fu, J. Lei, X. Song, W. S. Battaglia, W. Yang, P. B. Messersmith, G. Liu, *Nano Lett.* **2015**, *15*, 7927.
- [118] X. Wang, L. Lv, Z. Cheng, J. Gao, L. Dong, C. Hu, L. Qu, *Adv. Energy Mater.* **2016**, *6*, 1502100.
- [119] S. T. Kuk, A. Weichowski, *J. Power Sources* **2005**, *141*, 1.
- [120] H. Dong, J. P. Hinstroza, *ACS Appl. Mater. Interfaces* **2009**, *1*, 797.
- [121] J. Gu, F. Héroguel, J. Luterbacher, X. Hu, *Angew. Chem.* **2018**, *130*, 2993.
- [122] N. A. Kotov, I. Dékány, J. H. Fendler, *J. Phys. Chem.* **1995**, *99*, 13065.
- [123] J. Schmitt, G. Decher, W. J. Dressick, S. L. Brandow, R. E. Geer, R. Shashidher, J. M. Calvert, *Adv. Mater.* **1997**, *9*, 61.
- [124] Y. Ko, S. W. Ryu, J. Cho, *Appl. Surf. Sci.* **2016**, *368*, 36.
- [125] D. Buttry, *Advances in Electroanalytical Chemistry: Applications of the QCM to Electrochemistry*, Marcel Dekker, New York **1991**.
- [126] M. N. Hyder, B. M. Gallant, N. J. Shah, Y. Shao-Horn, P. T. Hammond, *Nano Lett.* **2013**, *13*, 4610.
- [127] S. W. Lee, J. Kim, S. Chen, P. T. Hammond, Y. Shao-Horn, *ACS Nano* **2010**, *4*, 3889.
- [128] S. W. Lee, B.-S. Kim, S. Chen, Y. Shao-Horn, P. T. Hammond, *J. Am. Chem. Soc.* **2009**, *131*, 671.
- [129] D. Nam, Y. Heo, S. Cheong, Y. Ko, J. Cho, *Appl. Surf. Sci.* **2018**, *440*, 730.
- [130] Z. Li, J. Wang, X. Liu, S. Liu, J. Qu, S. Yang, *J. Mater. Chem.* **2011**, *21*, 3397.
- [131] S. Kim, Y. Kim, Y. Ko, J. Cho, *J. Mater. Chem.* **2011**, *21*, 8008.
- [132] Y. Zhou, Z. Li, N. Hu, Y. Zeng, J. F. Rusling, *Langmuir* **2002**, *18*, 8573.
- [133] K. Jost, G. Dion, Y. Gogotsi, *J. Mater. Chem. A* **2014**, *2*, 10776.
- [134] J. J. Richardson, M. Björnmalm, F. Caruso, *Science* **2015**, *348*, aaa2491.
- [135] K. C. Krogman, N. S. Zacharia, S. Schroeder, P. T. Hammond, *Langmuir* **2007**, *23*, 3137.
- [136] A. T. Bell, *Science* **2003**, *299*, 1688.
- [137] L. Wang, H. Ji, S. Wang, L. Kong, X. Jiang, G. Yang, *Nanoscale* **2013**, *5*, 3793.
- [138] Y. Wang, H. Li, P. He, E. Hosono, H. Zhou, *Nanoscale* **2010**, *2*, 1294.
- [139] V. Pop, H. J. Bergveld, P. H. L. Notten, P. P. L. Regtien, *Meas. Sci. Technol.* **2005**, *16*, R93.
- [140] J. B. Goodenough, K.-S. Park, *J. Am. Chem. Soc.* **2013**, *135*, 1167.
- [141] H. Gwon, J. Hong, H. Kim, D.-H. Seo, S. Jeon, K. Kang, *Energy Environ. Sci.* **2014**, *7*, 538.



- [142] Y. Khan, A. E. Ostfeld, C. M. Lochner, A. Pierre, C. Arias, *Adv. Mater.* **2016**, *28*, 4373.
- [143] A. Yoshino, K. Sanekihika, T. Nakajima, *JP* 1989293, **1985**.
- [144] A. K. Padhi, K. S. Nanjundaswamy, J. B. Goodenough, *J. Electrochem. Soc.* **1997**, *144*, 1188.
- [145] J. Lu, Z. Chen, Z. Ma, F. Pan, L. A. Curtiss, K. Amine, *Nat. Nanotechnol.* **2016**, *11*, 1031.
- [146] H. Zhou, D. Li, M. Hibino, I. Honma, *Angew. Chem., Int. Ed.* **2005**, *44*, 797.
- [147] M. Okubo, E. Hosono, J. Kim, M. Enomoto, N. Kijima, T. Kubo, H. Zhou, I. Honma, *J. Am. Chem. Soc.* **2007**, *129*, 7444.
- [148] J. Wang, J. Polleux, J. Lim, B. Dunn, *J. Phys. Chem. C* **2007**, *111*, 14925.
- [149] P. He, Z. Zhang, Y.-G. Wang, L. Cheng, T.-Y. Xia, *J. Electrochem. Soc.* **2008**, *155*, A144.
- [150] M. Okubo, E. Hosono, J. Kim, M. Enomoto, N. Kojima, T. Kubo, H. Zhou, I. Honma, *J. Am. Chem. Soc.* **2007**, *129*, 7444.
- [151] D. Larcher, C. Masquelier, D. Bonnin, Y. Chabre, V. Masson, J. -B. Leriche, J.-M. Tarascon, *J. Electrochem. Soc.* **2003**, *150*, A133.
- [152] A. K. Rai, L. T. Anh, J. Gim, V. Mathew, J. Kang, B. J. Paul, J. Song, J. Kim, *Electrochim. Acta* **2013**, *90*, 112.
- [153] P. Yang, J.-M. Tarascon, *Nat. Mater.* **2012**, *11*, 560.
- [154] Y.-T. Liu, P. Zhang, N. Sun, B. Anasori, Q.-Z. Zhu, H. Liu, Y. Gogotsi, B. Xu, *Adv. Mater.* **2018**, *30*, 1707334.
- [155] L. Wang, D. Wang, Z. Dong, F. Zhang, J. Jin, *Nano Lett.* **2013**, *13*, 1711.
- [156] H. Wu, G. Yu, L. Pan, N. Liu, M. T. McDowell, Z. Bao, Y. Cui, *Nat. Commun.* **2013**, *4*, 1943.
- [157] Y. Wang, Y. Wang, E. Hosono, K. Wang, H. Zhou, *Angew. Chem., Int. Ed.* **2008**, *47*, 7461.
- [158] W.-M. Zhang, Z.-L. Wu, J.-S. , Hu, Y.-G. Guo, L.-J. Wan, *Adv. Funct. Mater.* **2008**, *18*, 3941.
- [159] D. Bresser, E. Paillard, R. Kloepsch, S. Krueger, M. Fiedler, R. Schmitz, D. Baither, M Winter, S. Passerini, *Adv. Energy Mater.* **2013**, *3*, 513.
- [160] D. Chen, X. Mei, G. Ji, M. Lu, J. Xie, J. Lu, J. Y. Lee, *Angew. Chem., Int. Ed.* **2012**, *51*, 2409.
- [161] S. Murugesan, J. T. Harries, B. A. Korgel, K. J. Stevenson, *Chem. Mater.* **2012**, *24*, 1306.
- [162] J. Jiang, Y. Li, J. Liu, X. Huang, C. Yuan, X. W. D. Lou, *Adv. Mater.* **2012**, *24*, 5166.
- [163] B.-L. He, B. Dong, H.-L. Li, *Electrochem. Commun.* **2007**, *9*, 425.
- [164] W. Wang, Y. Guo, L. Liu, S. Wang, X. Yang, H. Guo, *J. Power Sources* **2014**, *245*, 624.
- [165] C. Ban, Z. Wu, D. T. Gillaspie, L. Chen, Y. Yan, J. L. Blackburn, A. C. Dillon, *Adv. Mater.* **2010**, *22*, E145.
- [166] Y. Sun, X. Hu, J. C. Yu, Q. Li, W. Luo, L. Yuan, W. Zhang, Y. Huang, *Energy Environ. Sci.* **2011**, *4*, 2870.
- [167] C. Kim, J.-W. Jung, K. R. Yoon, D.-Y. Youn, S. Park, I.-D. Kim, *ACS Nano* **2016**, *10*, 11317.
- [168] C.-J. Bae, C. K. Erdonmez, J. W. Halloran, Y.-M. Chiang, *Adv. Mater.* **2013**, *25*, 1254.
- [169] G. A. Ferrero, A. B. Fuertes, M. Sevilla, *J. Mater. Chem. A* **2015**, *3*, 2914.
- [170] R. Dominko, J. M. Goupil, M. Bele, M. Gaberscek, M. Remskar, D. Hanzel, J. Jamnik, *J. Electrochem. Soc.* **2005**, *152*, A858.
- [171] Y. Ma, C. Fang, B. Ding, G. Ji, J. Y. Lee, *Adv. Mater.* **2013**, *25*, 4646.
- [172] P. Strubel, S. Thieme, T. Biemelt, A. Helmer, M. Oschatz, J. Brückner, H. Althues, S. Kaskel, *Adv. Funct. Mater.* **2015**, *25*, 287.
- [173] D. Y. W. Yu, K. Donoue, T. Inoue, M. Fujimoto, S. Fujitani, *J. Electrochem. Soc.* **2006**, *153*, A835.
- [174] J. M. D. Coey, A. E. Berkowitz, L. Balcells, F. F. Putris, F. T. Parker, *Appl. Phys. Lett.* **1998**, *72*, 734.
- [175] Z. Li, D. King, G. Zhou, S. Wu, W. Lv, C. Luo, J.-J. Shao, B. Li, F. Kang, Q.-H. Yang, *Energy Storage Mater.* **2017**, *6*, 98.
- [176] Y. Wang, Y. Li, Z. Qui, X. Wu, P. Zhou, T. Zhou, J. Zhao, Z. Miao, J. Zhou, S. Zhuo, *J. Mater. Chem. A* **2018**, *6*, 11189.
- [177] F. Han, D. Li, W. -C. Li, Q. Sun, A.-L. Lu, *Adv. Funct. Mater.* **2013**, *23*, 1692.
- [178] J. Liang, K. Xi, G. Tan, S. Chen, T. Zhao, P. R. Coxon, H.-K. Kim, S. Ding, Y. Yang, R. V. Kumar, J. Lu, *Nano Energy* **2016**, *27*, 457.
- [179] J. Han, D. Kong, W. Lv, D.-M. Tang, D. Han, C. Zhang, D. Liu, Z. Xiao, X. Zhang, J. Xiao, X. He, F.-C. Hsia, C. Zhang, Y. Tao, D. Golberg, F. Kang, L. Zhi, Q.-H. Yang, *Nat. Commun.* **2018**, *9*, 402.
- [180] T. Ma, X. Yu, H. Li, W. Zhang, X. Cheng, W. Zhu, X. Qiu, *Nano Lett.* **2017**, *17*, 3959.
- [181] Y. Zhu, S. Murali, M. D. Stoller, K. J. Ganesh, W. Cai, P. J. Ferreira, A. Pirkle, R. M. Wallace, K. A. Cychosz, M. Thommes, D. Su, E. A. Stach, R. S. Ruoff, *Science* **2011**, *332*, 1537.
- [182] M. Salanne, B. Rotenberg, K. Naoi, K. Kaneko, P. -L. Taberna, C. P. Grey, B. Bunn, P. Simon, *Nat. Energy* **2016**, *1*, 16070.
- [183] W. Wei, X. Cui, W. Chen, D. G. Lvey, *Chem. Soc. Rev.* **2011**, *40*, 1697.
- [184] J. P. Zheng, *J. Power Sources* **2004**, *137*, 158.
- [185] J. Xu, Q. Wang, X. Wang, Q. Xiang, B. Liang, D. Chen, G. Shen, *ACS Nano* **2013**, *7*, 5453.
- [186] L. Ma, H. Fan, X. Wei, S. Chen, Q. Hu, Y. Liu, C. Zhi, W. Lu, J. A. Zapien, H. Huang, *J. Mater. Chem. A* **2018**, *6*, 19058.
- [187] L. Hu, M. Pasta, F. L. Mantia, L. Cui, S. Jeong, H. D. Deshazer, J. W. Choi, S. M. Han, Y. Cui, *Nano Lett.* **2010**, *10*, 708.
- [188] K. Jost, C. R. Perez, J. K. McDonough, V. Presser, M. Heon, G. Dion, Y. Gogotsi, *Energy Environ. Sci.* **2011**, *4*, 5060.
- [189] V. Presser, L. Zhang, J. J. Niu, J. McDonough, C. Perez, H. Fong, Y. Gogotsi, *Adv. Energy Mater.* **2011**, *1*, 423.
- [190] Q. Huang, D. Wang, Z. Zheng, *Adv. Mater.* **2016**, *6*, 1600783.
- [191] D. Shin, C. H. Kwon, Y. Ko, B. Lee, S. W. Lee, J. Cho, *J. Mater. Chem. A* **2018**, *6*, 20421.
- [192] M. Chen, L. Zhang, S. Duan, S. Jian, H. Jiang, C. Li, *Adv. Funct. Mater.* **2014**, *24*, 7548.
- [193] C. Portet, P. L. Taberna, P. Simon, E. Flahaut, *J. Electrochem. Soc.* **2006**, *153*, A649.
- [194] D. Liang, S. Wu, J. Liu, Z. Tian, C. Liang, *J. Mater. Chem. A* **2016**, *4*, 10609.
- [195] Z. Hu, X. Xiao, C. Chen, T. Li, L. Huang, C. Zhang, J. Su, L. Miao, J. Jiang, Y. Zhang, J. Zhou, *Nano Energy* **2015**, *11*, 226.
- [196] X. Lu, G. Wang, T. Zhai, M. Yu, J. Gan, Y. Tong, Y. Li, *Nano Lett.* **2012**, *12*, 1690.
- [197] H.-S. Kim, J. B. Cook, H. Lin, J. S. Ko, S. H. Tolbert, V. Ozolins, B. Duun, *Nat. Mater.* **2017**, *16*, 454.
- [198] M. Dieterle, G. Weinberg, G. Mestl, *Phys. Chem. Chem. Phys.* **2002**, *4*, 812.
- [199] J.-Y. Shin, J. H. Joo, D. Samuelis, *Chem. Mater.* **2012**, *24*, 543.
- [200] C. Choi, D. S. Ashby, D. M. Butts, R. H. DeBlock, Q. Wei, J. Lau, B. Duun, *Nat. Rev. Mater.* **2020**, *5*, 5.
- [201] N. Liu, W. Ma, J. Tao, X. Zhang, J. Su, L. Li, C. Yang, Y. Gao, D. Golberg, Y. Bando, *Adv. Mater.* **2013**, *25*, 4925.
- [202] J. Sun, Y. Huang, C. Fu, Y. Huang, M. Zhu, X. Tao, C. Zhi, H. Hu, *J. Mater. Chem. A* **2016**, *4*, 14877.
- [203] Y. Li, X. Yan, X. Zheng, H. Si, M. Li, Y. Liu, Y. Sun, Y. Jiang, Y. Zhang, *J. Mater. Chem. A* **2016**, *4*, 17704.
- [204] Z. Zhang, F. Xiao, S. Wang, *J. Mater. Chem. A* **2015**, *3*, 11215.
- [205] H. Zu, X. Hu, Y. Sun, H. Yang, X. Liu, Y. Huang, *Nano Res.* **2015**, *8*, 1148.
- [206] J. Yu, W. Lu, J. P. Smith, K. S. Booksh, L. Meng, Y. Huang, Q. Li, J.-H. Byun, Y. Oh, Y. Yan, T.-W. Chou, *Adv. Energy Mater.* **2017**, *7*, 1600976.
- [207] Y. Huang, H. Hu, Y. Huang, M. Zhu, W. Meng, C. Liu, Z. Pei, C. Hao, Z. Wang, C. Zhi, *ACS Nano* **2015**, *9*, 4766.

- [208] X. Pu, L. Li, M. Liu, C. Jiang, C. Du, Z. Zhao, W. Hu, Z. L. Wang, *Adv. Mater.* **2016**, *28*, 98.
- [209] S. Stauss, I. Honma, *Bull. Chem. Soc. Jpn.* **2018**, *91*, 492.
- [210] A. T. Yahiro, S. M. Lee, D. O. Kimble, *Biochim. Biophys. Acta.* **1964**, *88*, 375.
- [211] S. Cosnier, A. L. Goff, M. Holzinger, *Electrochem. Commun.* **2014**, *38*, 19.
- [212] A. J. Bandodkar, J.-M. You, N.-H. Kim, Y. Gu, R. Kumar, A. M. V. Mohan, J. Kurniawan, S. Imani, T. Nakagawa, B. Parish, M. Parthasarathy, P. P. Mercier, S. Xu, J. Wang, *Energy Environ. Sci.* **2017**, *10*, 1581.
- [213] A. J. Bandodkar, *J. Electrochem. Soc.* **2017**, *164*, H3007.
- [214] C. H. Kwon, S.-H. Lee, Y.-B. Choi, J. A. Lee, S. H. Kim, H.-H. Kim, G. M. Spinks, G. G. Wallace, M. D. Lima, M. E. Kozlov, R. H. Baughman, S. J. Kim, *Nat. Commun.* **2014**, *5*, 3928.
- [215] V. Coman, R. Ludwig, W. Harreither, D. Haltrich, L. Gorton, T. Ruzgas, S. Shleev, *Fuel Cells* **2010**, *10*, 9.
- [216] F. Gao, L. Viry, M. Maugey, P. Poulin, N. Mano, *Nat. Commun.* **2010**, *1*, 2.
- [217] A. Zebda, C. Gondran, A. L. Goff, M. Holzinger, P. Cinquin, S. Cosnier, *Nat. Commun.* **2011**, *2*, 370.
- [218] U. Salaj-Kosla, M. D. Scanlon, T. Baumeister, K. Zahma, R. Ludwig, P. Ó. Conghaile, D. MacAodha, D. Leech, E. Magner, *Anal. Bioanal. Chem.* **2013**, *405*, 3823.
- [219] H. Sakai, T. Nakagawa, Y. Tokita, T. Hatazawa, T. Ikeda, S. Tsujimura, K. Kano, *Energy Environ. Sci.* **2009**, *2*, 133.
- [220] A. Heller, *Curr. Opin. Chem. Biol.* **2006**, *10*, 664.
- [221] P. Kavanagh, D. Leech, *Phys. Chem. Chem. Phys.* **2013**, *15*, 4859.
- [222] Y. Xiao, F. Patolsky, E. Katz, J. F. Hainfeld, I. Willner, *Science* **2003**, *299*, 1877.
- [223] A. Heller, *Nat. Biotechnol.* **2003**, *21*, 631.
- [224] X. Xie, W. Xu, X. Liu, *Acc. Chem. Res.* **2012**, *45*, 1511.
- [225] O. Yehezkeili, R. Tel-Vered, S. Raichlin, I. Willner, *ACS Nano* **2011**, *5*, 2385.
- [226] I. W. Schubart, G. Göbel, F. Lisdat, *Electrochim. Acta* **2012**, *82*, 224.
- [227] L. Wang, Z. Tang, W. Yan, H. Yang, Q. Wang, S. Chen, *ACS Appl. Mater. Interfaces* **2016**, *8*, 20635.
- [228] V. Krikstolaityte, A. Barrantes, A. Ramanavicius, T. Arnebrant, S. Shleev, T. Ruzgas, *Bioelectrochemistry* **2014**, *95*, 1.
- [229] F. Caruso, D. Trau, H. Möhwald, R. Renneberg, *Langmuir* **2000**, *16*, 1485.
- [230] A. Yu, Z. Liang, J. Cho, F. Caruso, *Nano Lett.* **2003**, *3*, 1203.
- [231] A. Yu, Y. Wang, E. Barlow, F. Caruso, *Adv. Mater.* **2005**, *17*, 1737.
- [232] A. Yu, Z. Liang, F. Caruso, *Chem. Mater.* **2005**, *17*, 171.
- [233] K. H. Hyun, S. W. Han, W.-G. Koh, Y. Kwon, *J. Power Sources* **2015**, *286*, 197.
- [234] E. Laviron, *J. Electroanal. Chem. Interfacial Electrochem.* **1979**, *101*, 19.
- [235] C. Cai, J. Chen, *Anal. Biochem.* **2004**, *332*, 75.
- [236] S.-J. Bao, C. M. Li, J.-F. Zang, X.-Q. Cui, Y. Qiao, J. Guo, *Adv. Funct. Mater.* **2008**, *18*, 591.
- [237] K. Murata, K. Kajiya, N. Nakamura, H. Ohno, *Energy Environ. Sci.* **2009**, *2*, 1280.
- [238] Y. Yan, W. Zheng, L. Su, L. Mao, *Adv. Mater.* **2006**, *18*, 2639.
- [239] P. Gai, Y. Ji, Y. Chen, C. Zhu, J. Zhang, J.-J. Zhu, *Analyst* **2015**, *140*, 1822.
- [240] C. Pan, Y. Fang, H. Wu, M. Ahmad, Z. Luo, Q. Li, J. Zie, Z. Yan, L. Wu, Z. L. Wang, J. Zhu, *Adv. Mater.* **2010**, *22*, 5388.
- [241] C. Chen, L. Wang, Y. Tan, C. Qin, F. Xie, Y. Fu, Q. Xie, J. Chen, S. Yao, *Biosens. Bioelectron.* **2011**, *26*, 2311.
- [242] P. Mishra, G. B. V. S. Lakshmi, S. Mishra, D. K. Avasthi, H. C. Swart, A. P. F. Turner, Y. K. Mishra, A. Tiwari, *Nano Energy* **2017**, *39*, 601.
- [243] Y. Chung, M. Christwardana, D. C. Tannia, K. J. Kim, Y. Kwon, *J. Power Sources* **2017**, *360*, 172.
- [244] I. Cho, B. J. Kim, S. W. Ryu, J. H. Cho, J. Cho, *Nanotechnology* **2014**, *25*, 505604.
- [245] S. Bae, H. Kim, Y. Lee, X. Xu, J.-S. Park, Y. Zheng, J. Balakrishnan, T. Lei, H. R. Kim, Y. I. Song, Y.-J. Kim, K. S. Kim, B. Özyilmaz, J.-H. Ahn, B. H. Hong, S. Iijima, *Nat. Nanotechnol.* **2010**, *5*, 574.